QATAR UNIVERSITY

COLLEGE OF ARTS AND SCIENCES

THE EFFECT OF SINGLE WALLED CARBON NANOTUBES ON THE THERMOELECTRIC PROPERTIES OF BISMUTH TELLURIDE

BY

MOHAMED ALAMELDIN ALI MOHAMED

A Thesis Submitted to

the College of Arts and Sciences

in Partial Fulfillment of the Requirements for the Degree of

Masters of Science in Material Science and Technology

January 2022

COMMITTEE PAGE

The members of the Committee approve the Thesis of
Mohamed Alameldin Ali Mohamed defended on 01/12/2021.

_____
Dr. Khaled Youssef
Thesis/Dissertation Supervisor

_____
Dr. Mohamed Hassan
Committee Member

_____
Dr. Ahmed Abdala
Committee Member

Approved:

_____
Ahmed Elzatahry, Dean, College of Arts and Sciences

ABSTRACT

MOHAMED, MOHAMED, A., Masters:

January: 2022, Material Science and Technology

Title: The effect of Single Walled Carbon Nanotubes on the Thermoelectric Properties of Bismuth Telluride

Supervisor of Thesis: Dr. Khaled Youssef.

Modern new technologies, including carbon nanomaterials, polymers performed electronically, and their nanocomposites enhance the performance of thermoelectric materials. Thermoelectrical responses can be improved by simultaneously tuning different properties within the material, such as nano structuring, nanocomposites, and doping. The purpose of this work is to determine the effect of single walled carbon nanotubes (SWCNT) on the thermoelectric properties of an n-type bismuth telluride alloy. Mechanical alloying and compaction sintering techniques are used to prepare SWCNT/$Bi_2Te_{2.55}Se_{0.45}$ composites. Experiments are conducted with different concentrations (0.01, 0.025, 0.1 and 0.5 weight percent) and duration times of 20 hours. The results of the thermoelectric characteristics of SWCNT indicates that ball milling technique influences both its structure and agglomeration. The CNT filler is added during the step of mechanical milling, as this preserves SWCNT structure and increases its electrical conductivity. Additionally, it is demonstrated that SWCNT milling technique improves the Seebeck coefficient. While an increase in thermal conductivity is expected as a result of the high electrical conductivity due to increased scattering at the new interfaces, a significant drop in the lattice thermal conductivity is attained. The figure-of-merit for the optimal sample with 0.1 percent SWCNT added in 20 milling hours has improved by 13% at room temperature indicating a value of 0.3, and by 32% at 156.9°C indicating the highest ZT value of 0.6.

DEDICATION

To my parents, who have been a consistent source of encouragement and support throughout my academic career and endless source of aspirations for my future.

ACKNOWLEDGMENTS

I would like to express my gratitude to Dr. Khaled Youssef, my thesis supervisor, for providing me with the opportunity to complete my thesis under his supervision, as well as for his ongoing academic guidance and support throughout my academic career. Ms. Farah M. El-Makaty deserves special credit for all the support given during the thesis experimental work and the endless sharing of information and knowledge. In addition, I would like to express my gratitude to the members of my thesis committee, Dr. Ahmed Abdala and Dr. Mohammad Hassan, for their comments and recommendations. They have all been helpful. I would like to express our gratitude to the Center for Advanced Materials and the Central Laboratory Unit at Qatar University for assisting me with the experimental work. Final words of thanks to the faculty members of the Materials Science and Technology Master Program, who have provided me with many useful courses throughout my Master of Science studies. I am grateful to them all.

TABLE OF CONTENTS

LIST OF TABLES

LIST OF FIGURES

CHAPTER 1: INTRODUCTION

1.1 Thermoelectric Materials

By converting waste heat to electrical energy without the use of bulk fluids or moving parts, thermoelectric materials can help reduce energy usage. A thermoelectric device is typically composed of two conducting materials connected via a junction. Conducting materials are classified as n-type or p-type based on whether they have negative or positive charge carriers (e.g., electrons, holes). Once a temperature gradient (ΔT) is established between the device's opposite ends, carriers diffuse from hot side (i.e., high thermal energy regime) to cold side (i.e., low thermal energy regime), resulting in the generation of electricity (Figures 1 and 2). The electric potential generated because of the temperature differential is referred to the phenomenon is well-known as Seebeck effect. Bismuth telluride, lead telluride, sodium cobaltate, tin selenide, and silicon germanium are the most well-known thermoelectric materials examples. They are utilized in lasers, computer chips, and infrared detectors. However, due to the low efficiency of commercial thermoelectric materials, their application is severely limited (Jaldurgam et al., 2021; Kasap et al., 2007; Yu et al., 2016).

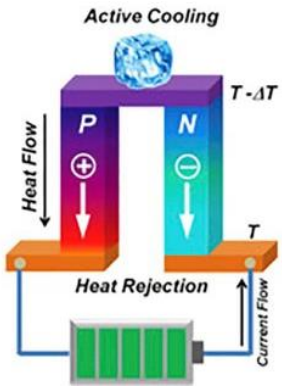

Figure 1. Schematic illustration of the thermoelectric active cooling mode (Yu et al., 2016).

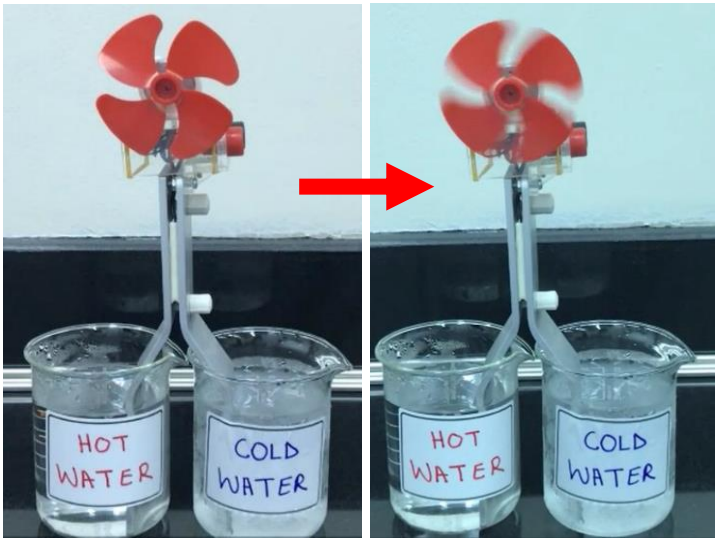

Figure 2. Thermoelectric fan operating with a temperature gradient (ΔT).

Over the last 200 years, the essential concepts of thermoelectricity have been established. Superior thermoelectric materials need a thorough understanding of electron and phonon transport processes in such materials. Inorganic materials have long been employed in thermoelectric research. Clathrates, half-Heusler (HH) alloys, Si–Ge alloys, rare earth chalcogenides (e.g., La3-xTe4), telluride-based materials (e.g., PbTe, Bi2Te3, etc.), and skutterudites are some examples. Recently, new types of materials have been suggested, including carbon nanomaterials, electrically conducting polymers and carbon nanomaterial/polymer nanocomposites. Figure 3 depicts the proportion contribution of various materials to thermoelectric technology (Gayner & Kar, 2016; Goel & Thelakkat, 2020; Li et al., 2021; Yao et al., 2019).

Modern new technologies, including carbon nanomaterials, polymers performed electronically, and their nanocomposites enhance the performance of thermoelectric materials. Thermoelectrical responses can be improved by simultaneously tuning different properties within the material, such as nano structuring, nanocomposites, and doping. Recent patterns have been identified for thermo-electric

research to suggest the suitability for electrical and energy sustainability of high-performance thermoelectric materials such as inorganic materials and carbon nanomaterials/ electronically conductive nanocomposite polymers (Jaldurgam et al., 2021; Shi et al., 2020).

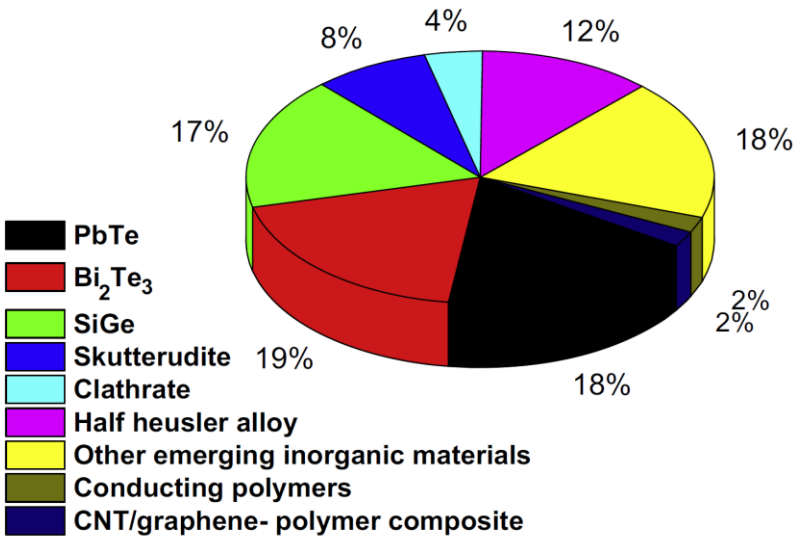

Figure 3: Individual contribution of various thermoelectric materials (Yao et al., 2019).

Bismuth telluride chalcogenides are suitable for use in near-room temperature thermoelectric materials applications. However, due to their incredibly poor heat conversion efficiency, the use of these materials is limited to few applications. The main aim of the research study, therefore, is to synthesis and develop a high performance, effective thermoelectric n-type bismuth telluride with carbon nanotubes (CNT) of different compositions and a thermoelectric value of Figure of Merit above 1. CNT will be used as a nanofiller in the preparation of the bismuth telluride nanocomposite. The samples will be treated with varying amounts of CNT and additional periods using ball milling techniques. The influence of CNT on the

thermoelectric properties of bismuth telluride will then be studied (Dresselhaus et al., 2007; Ju et al., 2019).

1.2 Properties of Thermoelectric Materials

The perfect thermoelectric material must demonstrate a small thermal conductivity, a large Seebeck coefficient, and a large electrical conductivity. The small thermal conductivity ensures high-temperature gradient, the large Seebeck coefficient confirms the high thermal voltages, and the Joule heating effect is reduced with the large electrical conductivity. Bismuth telluride chalcogenides are suitable for use in near-room temperature thermoelectric materials applications. However, due to their incredibly poor heat conversion efficiency, the use of these materials is limited to few applications. That is why the main aim of the research study is to synthesis and develop a high-performance thermoelectric bismuth telluride with carbon nanotubes (CNT) of different compositions (Deng & Liu, 2009).

The effectiveness of thermoelectric materials in converting energy is based on their physical transport qualities, which can be determined using the dimensionless Figure-of-Merit (ZT). as specified in Equation (Shin et al., 2017).

$$ZT = \frac{S^2 \sigma T}{\kappa} \quad (1)$$

This dimensionless variable is conditional on the Seebeck coefficient(S), the electrical conductivity (σ), the absolute temperature (T) at which these physical parameters are determined, and the overall thermal conductivity. The overall thermal conductivity is calculated by adding the electronic(κ_E) and lattice (κ_L) thermal conductivities; The thermoelectric power factor is denoted by the symbol $S^2\sigma$ (Ahmad & Wan, 2017; Tong, 2011).

1.2.1 Electrical Conductivity

The electrical conductivity of TE materials directly based mainly on the charge carrier concentration (n), charge carrier mobility (μ) and charge of the carrier (e), all of which are affected by the material's electrical band structure, as displayed in Equation (2):

$$\sigma = ne\mu (2)$$

Additionally, as stated in equation (3) below, mobility of charge carriers is composed of the mobility of carriers at the interface ($\mu_{interface}$) and the mobility of carriers in the matrix (μ_{matrix})

$$\frac{1}{\mu_{Total}} = \frac{1}{\mu_{matrix}} + \frac{1}{\mu_{interface}} (3)$$

And The term "interface mobility" ($\mu_{interface}$) refers to the following:

$$\mu_{interface} = Le(\frac{1}{2\pi m^* k_B T})^{\frac{1}{2}} \exp\left(-\frac{E_B}{k_B T}\right) (4)$$

where *kB, m*, L, T, and EB denote, respectively, the Boltzmann constant,* the charge carriers effective mass which depend on band structure of TE material, The distance between two adjacent interfaces is denoted by the letter L, absolute temperature, EB the height of a potential barrier (Kumar et al., 2018).

As a result of equation (4), it has been observed that elevated temperatures reduce mobility at the interface, hence decreasing total mobility of charge carrier (μ_{Total}).

1.2.2 Seebeck Coefficient

In contrast to electrical conductivity (σ), the term Seebeck coefficient (S) is inversely proportional to charge carrier concentration (n), as seen in equation (5):

$$S = \frac{8\,\pi^2 k_B^2}{3\,e\,h^2}\; m^* T(\frac{\pi}{3n})^{\frac{2}{3}} \quad (5)$$

The Planck's constant is denoted by the letter h (Ju et al., 2016). As a result, the preceding two thermoelectric parameters typically have the opposite effect on the TE material.

1.2.3 Thermal Conductivity

The total thermal conductivity (k) of TE materials is composed of the lattice phonon contribution (kL) and the electronic (kE) thermal conductivities and may be computed using the material's density (ρ), thermal diffusivity (D), and specific heat (Cp) values As for Equation 6:

$$k_{Total} = k_E + k_L = D\rho C_p \quad (6)$$

In addition, Wiedemann-Franz law identified the electronic thermal conductivity (kE) of the electric charge carriers:

$$k_E = \sigma TL \quad (7)$$

Where L is the Lorenz number, which ranges between 1.50 and 2.44*10-8 W.Ω.K-2 for non-degenerated and strongly degenerated semiconductors (Zhang et al., 2017).

Increasing the figure of merit can be accomplished by increasing the power factor value and/or decreasing total thermal conductivity ($S^2\sigma$). Despite extensive research on thermoelectric materials, the figure of merit value of commercially available materials is quite low, making Bi2Te3 alloys important for near-room-temperature applications (Kanatzidis, 2010). Mechanical Ball milling is a relatively inexpensive and widely applicable technology for nano structuring that has been shown to boost the ZT value (Mamur et al., 2018a).

The main objective of this work is to study the effect of SWCNT with different compositions on thermoelectric material performance of n-type Bismuth Telluride (Bi_2Te_3) to achieve a thermoelectric Figure of merit above 1. In addition, the study aims

to stabilize the synthesized nanocomposite for long-term operation and to examine the influence of CNT on the thermoelectric properties of bismuth telluride. To achieve this, SWCNT is integrated into a $Bi_2Te_{2.55}Se_{0.45}$ bulk materials matrix system based on molecular level mixing to improve its mechanical and thermoelectric characteristics as a function of temperature using a powder processing approach. High intensity ball milling and compaction methods are used to successfully manufacture nanocrystalline CNT/$Bi_2Te_{2.55}Se_{0.45}$ composites. X-ray Diffraction (XRD), Scanning Electron Microscope (SEM), and Transmission Electron Microscopy (TEM) analytical methods are used to study the structural characterization and average grain size of both $Bi_2Te_{2.55}Se_{0.45}$ pristine and CNT/$Bi_2Te_{2.55}Se_{0.45}$ system. The mechanical and thermal characteristics of $Bi_2Te_{2.55}Se_{0.45}$ are studied using the Vicker microhardness test as the quantity of SWCNT is raised. At different temperatures, the Seebeck coefficient and electrical conductivity are both measured concurrently in the SBA 458 Nemesis system. The Light Flash Apparatus LFA 467 HyperFlash is used to measure thermal conductivity. The obtained results demonstrates the effectiveness of SWCNT/$Bi_2Te_{2.55}Se_{0.45}$ nanostructured composite manufacturing with increased thermoelectric performance and a high Seebeck coefficient.

The research questions and hypothesis aimed to be resolved in this study are highlighted in the following points:

1. How do nanostructuring and doping contribute to influence the thermoelectric properties of bismuth telluride?
2. What is the optimum concentration of SWCNT that can give the highest ZT of bismuth telluride?

CHAPTER 2: LITERATURE REVIEW

2.1 History of Thermoelectric Materials

Around 70% of the energy generated in the world is projected to be primarily waste heat rejected into the atmosphere. A sustainable, economical, and effective way to recycle part of waste heat will have a significant effect on total renewables output and carbon footprint reduction. Thermoelectric materials can minimize energy consumption without the need for transporting fluids and components by turning waste heat into electrical energy. A standard thermoelectric device consists of the interaction of two conduction materials. One substance has a negative load carrier (e.g., electron) and is known as n-type, whereas the other has a positive load carrier (such as holes) and is called p-type. Where a temperature differential is imposed at the opposite ends of the unit, the transportation networks can distribute energy from the warm to the cold (Figure 4). This energy is generated by the electricity produced by the Seebeck coefficient. There are compact scale, lightweight, and noise-free benefits of thermoelectric instruments. In many applications, however, the poor efficiencies of industrial thermoelectric materials limit their use (Nozariasbmarz et al., 2020).

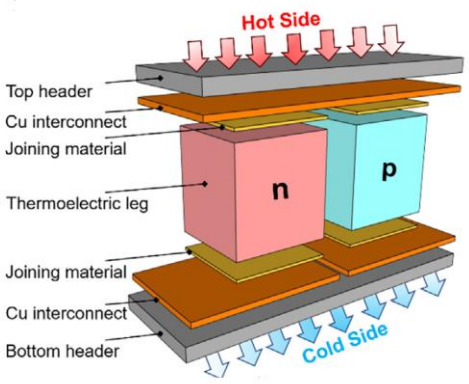

Figure 4: Customized single couple thermoelectric generator module

In green energy conversion technology, thermoelectric materials are critical for addressing the global energy challenge. They have proved to be sufficient for technologically sophisticated applications such as rockets and spacecraft. Human beings are facing a large rise in energy consumption. Renewable resources of energy are important for addressing the energy problems in the future with the decline of fossil fuels. The technology for energy conversions, such as solar panels and fuel cells, is highly important in this regard, while their global commercialization is constrained by their poor long-term stability, high costs, and low performance. For the direct conversion of heat to electricity, thermoelectric machines are used. These systems are typically capable of using any thermal source, including solar and waste heat. The production of renewable energy-efficient technology, therefore needs thermoelectric materials to play a key role. Moreover, these Thermoelectric Appliances are free of friction and noise and have no moving components. The thermoelectric efficiency of the machinery depends primarily on the form and properties of the materials used, such as their thermal stability, heat conductivity, electric conductivity, and Seebeck coefficient. Due to its enhanced thermoelectric responses compared to organic materials, classical inorganic substances have become important (Gayner & Kar, 2016; Goel & Thelakkat, 2020; Li et al., 2021; Yao et al., 2019).

The Seebeck method was first developed in 1821. The Peltier effect first discovered in 1834. Gustav Magnus claimed in 1851 that the potential difference between two thermocouple connections is proportional to the applied temperature difference. This effect was experimentally proven in 1856 (Androulakis et al., 2006). 1940s: Altenkirch coined the phrase “thermoelectric figure of merit” ZT. He recommended a thermoelectric material with a high Seebeck coefficient (S), low thermal conductivity (k), and a large electrical conductivity to minimize Joule heating.

Bloch demonstrated that thermal vibration of the lattice and impurities affect metal electrical conductivity (σ). Wilson proposed that the conductivity of semiconductors and insulators be temperature dependent. Low carrier concentration reduces conductivity at low temperatures (Kanatzidis, 2010). 1950- 1959: Ioffe stated that (k) of semiconductors is atomic weight dependent. Massive elements have low thermal conductivity (however low (k) has been observed in low-density materials) . Horovitz suggested a model for low-temperature lattice equilibrium deviations (Bulusu & Walker, 2008; Goldsmid, 2010; Rowe, 2018). Goldsmid investigated the relationship between heat conductivity and electron mobility (Goldsmid, 2010). Goldsmid proposed that electron mobility is a function of atomic weight. It was hypothesized by Ioffe that alloying semiconductors with isomorphous materials would diminish their heat (k) without altering their electrical conductivity. So thermoelectric applications employed modified semiconductor alloys. In this regard, Ioffe introduced figure of merit (ZT) as a thermoelectric performance metric (Bulusu & Walker, 2008; Goldsmid, 2010; Rowe, 2018).1960-1969.

The material parameter (fit parameter) relates carrier mobility, effective mass, doping, temperature, and (k) (Chasmar & Stratton, 1959). Ioffe's model shows the effect of bandgap on ZT. This contributes to the excessive thermal conductivity (k) and poor carrier mobility. Based on irreversible thermodynamics, Littman and Davidson hypothesized no ZT upper limit. The existence of multiple orientations/interfaces affects thermal conductivity due to phonon scattering, as mentioned by Dresselhaus and Hicks in 1970–2015. Thus, the alternating barrier layers of superlattices have finite thermal conductivity and tunneling probability in quantum wells. They projected a rise in ZT, but below that predicted by Dresselhaus and Hicks (Dresselhaus et al., 2007; Hicks & Dresselhaus, 1993a, 1993b). Both Bulusu and Walker suggested that

nonequilibrium Green's function approach for determining the thermoelectric performance of Si/Ge/Si superlattices. Quantum effects are modelled using sub-band dispersion relations. Also investigated the effects of confinement and scattering on superlattice electrical conductivity (σ) and (S) (Bulusu & Walker, 2008). Among bulk thermoelectric materials (TE), new classes of materials have been proposed to reduce thermal conductivity and increase power factor (PF) such as (PbTe, Bi2Te3, etc.) (Hsu et al., 2004; Quarez et al., 2005; Slack & Tsoukala, 1994; Zhou et al., 2008). Slack suggested a model with atoms in a cage-like shape and the ''PGEC" concept (Slack & Tsoukala, 1994). Heremans, Snyder, and others studied semiconductor strategies for enhancing the (TE) eg. doping and its effect on thermoelectric response. These include energy filtering, energy level pining, multiple-band conduction methods, and electronic band convergence as new concept (Heremans et al., 2008). Initial research focused on innovative thermoelectric materials. A panoscopic technique combining band engineering and nanostructuring was proposed by Biswas et al. (2012). Other groups research and Ran they achieved high ZT values for low-temperature (e.g.,Bi2Te3) and high-temperature (HH alloys) materials using the same combination (Makongo et al., 2011). A panoscopic approach involving hierarchical scattering of phonons, via atomic-scale lattice disorders and nanoscale endotaxial precipitates to mesoscale grain boundaries (Biswas et al., 2012); nanostructure engineering; band structure engineering; and a synergistic approach of high-mobility electrons have all been introduced (Xie et al., 2013). Thermoelectric response of materials can be improved by nanostructuring, doping, or using nanocomposites. The present research study to create flexible (TE) using electronic polymers and Thermoelectric devices with great performance and low weight different carbon nanomaterials are also being developed (He et al., 2013).

2.2 Bismuth Telluride as a Thermoelectric Material

Bismuth telluride (Bi_2Te_3) alloys have been recognized early and developed since the 1960s, which crystallizes in a rhombohedral crystal structure with a bandgap of 0.15 eV. It consists of repeating quintuple layers block in the sequence of Te(1)-Bi-Te(2)-Bi-Te2(1) presented in Figure 5. The bonds between Te and Bi atoms are tightly covalent, while van der Waals interactions are bonded to the corresponding Te atoms. These alloys are one of the most key systems used for applications with low temperatures, typically below 250 ^oC. At room temperature, Bi_2Te_3 demonstrate a good thermoelectric material. The unit cell parameters of this semiconductor have a lattice constant a = 3.8 Å and c = 30.5 Å, respectively. The ability to preserve its symmetry with doping is one feature of this system. Doping Bi_2Te_3 semiconductor with antimony (Sb) or selenium (Se) gives either hole or electron conducting thermoelectric materials. For Bismuth telluride alloys, the improved compositions for the p- and n- types are $Bi_{0.5}Sb_{1.5}Te_3$ and $Bi_2Te_{2.7}Se_{0.3}$, respectively (An et al., 2019; Manzano et al., 2016; Neeli et al., 2016; Park et al., 2015; Tritt & Subramanian, 2006).

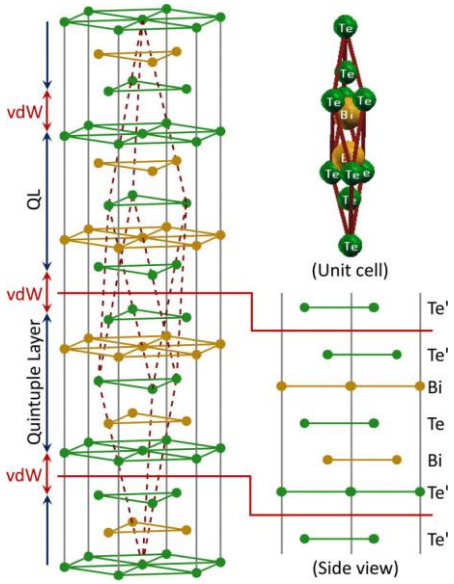

Figure 5: Crystal structure of bismuth telluride

2.3 Strategies for Enhancing Thermoelectric Performance

2.3.1 Nano-structuring

Nanostructures are referred to as materials that have at least one dimension in the 1 and 100 nm range. Nanostructures give materials exclusive and unique characteristics while retaining their bulk properties. Nanomaterials offer a wide range of applications because of the high surface area of these structures. Since they play a crucial role in the development of technologies, recent years have seen an increase in study interest in nanostrucuring approach in electrical, chemical, biological, physical, and optoelectrical domains. At the nanoscale, unique properties are created because of electron confinement in space, and they are highly dependent on the material's size. Bismuth telluride alloys have recently had their thermoelectric characteristics improved via nanostructuring, resulting in a significant increase in their figure-of-merit (ZT) (Mamur et al., 2018a).

The increased density of grain boundaries and interfaces inside nanostructured bulk TE is responsible for the increase in figure-of-merit (ZT) values. These are critical for improving phonon scattering by lowering the lattice thermal conductivity and thus increasing the ZT value. In general, there are two nanostructuring methods, either top-down or bottom-up. The first method depends on the division into the nanoscale of a bulk substance, while the latter method builds up the material by binding atoms or molecules together. Numerous investigations have already examined the characteristics of Bi2Te3 TE generated in this manner. Takashiri et al. (2007), for example, created nanocrystalline thin films of n-type bismuth telluride via a bottom-up process called flash evaporation.

Fan et al. (2010) studied the impact of nano-inclusions as a top-down approach on the ZT value of (Bi2Te3) nanocomposites prepared by melt spinning. Thermal conductivity was lowered by 50% in comparison to the bulk material in the produced

films. Additionally, Fan et al. (2011) investigated the effect of nanoinclusions on the figure of merit value of (Bi2Te3) nanocomposites generated using top-down melt spinning. Increasing the weight of nano-inclusions inside the thermoelectric material has been shown by research groups to decrease its thermal conductivity (K) and therefore maintains a higher ZT value.

2.3.2 Nano-compositing

Compositing is the process of homogenizing disparate components to create a single material without physical blending. The developed substance possesses a unique combination of properties not found in any of the individual materials.in general Composite materials are typically made up of a matrix and a filler material. It has been demonstrated that composites improve the thermoelectric characteristics of materials. Additionally, it has been reported that employing various fillers in combination with (Bi2Te3) as a matrix result in a decrease in the lattice thermal conductivity (kl) (Lognoné & Gascoin, 2015). This reduction is a result of the formation of new interfaces between the filler and the matrix material. Additionally, it has been claimed that these interfacial areas boost the Seebeck coefficient (S) value via carrier filtering or quantum confinement methods (Kim et al., 2013).

2.3.3 Doping

Doping It is the main band engineering strategy as it has demonstrated benefits for the improvement of thermoelectric material performance of the Bismuth telluride system (Xie et al., 2009) nanostructured. Doping changes, the concentration of the carrier concentration (n), increases Seebeck coefficient (S), introduces defects into Bi2Te3 nanocrystalline powder, and reduces thermal conduction (k). The dopant element is selenium (se), a standard dopant of Bi2Te3 n-type Improving the ZT.

2.3.4 Alloying

In a complex material system, alloy elements differ from the doping effect in the performance of thermoelectric materials. Allegation (alloying)increases the power factor (S2σ) while the thermal conductivity(k_E)is reduced for instance In most HH alloys and in skutterudits and clathrates these effects are ideally observed (Slack & Tsoukala, 1994). Alloying process elements can cause atomic disorder via induced atomic fluctuation or strain field effect, lowering lattice KE (Shen et al., 2001; Yang et al., 2008).

2.3.5 Nano-fillers

Mostly all fillers utilized in the fabrication of semiconductor TE are small, less than100nm in size, as they enable fine-tuning of the thermoelectric characteristics when they are controlled and managed at the nanoscale. Additionally, depending to the number of nanoscale dimensions of a material, nanofillers are classified as 1D, 2D, or 0 D materials. The filler shape, size, quantity, distribution, and orientation within the matrix can all have an effect on the alloy's thermoelectric characteristics. Quantum dots are zero-dimensional fillers; the quantum wire is a two-dimensional filler; and quantum wire is a one-dimensional filler, depending on their nanoscale size. Graphene sheets and graphene powders are the most often utilized (2DFs) fillers and have grown in popularity as a research subject since their successful isolation (Anno et al., 2015). Silicon carbide SiC and zirconium oxide ZnO are used as zero-dimensional fillers (0DFs). As one-dimensional fillers (1DFs), multi or single-wall carbon nanotubes are the most frequently employed.

2.4 Ball Milling

Ball milling, which uses mechanical energy to grind and refine the materials into smaller parts, is a top-down nanostructuring technique. It is found an effective dry powder processing approach for manufacturing nano-size alloys and solid solutions.

Even so, the main objective of the method of machine milling (MM) is a grain refining or phase transformation. As shown in Figure 6, grain refinement happens as a consequence of extreme plastic deformation from repetitive mechanical impacts. Milling must be carried out until the time required to achieve a steady-state of the starting materials. Then, by heat treatments, the resulting powder is compacted into a bulk in order to examine and analyze and obtain the desired microstructure and features. The initial raw materials, the mechanical mill, and the system parameters utilized are the main components of the MM process.

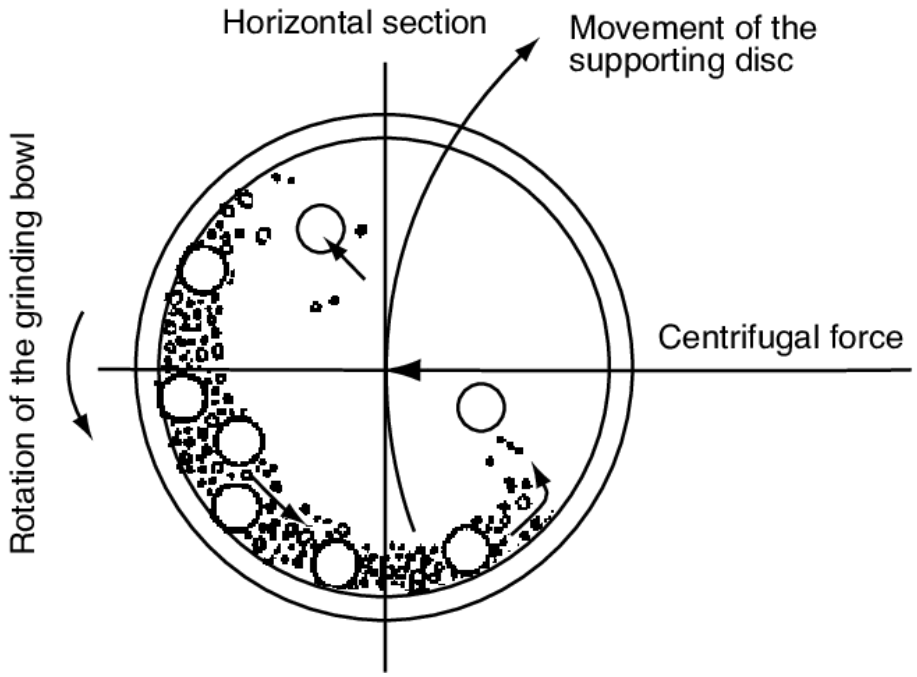

Figure 6: Dynamics of Ball Milling

Metals, alloys, or refractory materials may be part of the initial raw powder. Their size can vary from 1-200 μm, but the basic powder size must be smaller than the grinding medium (e.g. grinding balls), most significantly. It is important to use high purity powders as these determine the product's final structure, phase, and kinetics (Suryanarayana, 2001)). It is noted that the nanomaterials developed by ball milling appear to reduce thermal conductivity while keeping strong electron transport characteristics in many research studies (Suh et al., 2015). Ball milled goods are often

shown to increase the power factor, which helps to improve the Figure of merit value comparison to standard bulk materials in exchange (Mamur et al., 2018b).

2.5 Carbon Nanotubes

Numerous fillers are used for compositing thermoelectric semiconductor materials as they provide a nanoscale (< 100 nm) regulated ability to change the thermoelectric properties. In addition, nanofillers are divided into various classes by the number of dimensions of a substance that is in the nanoscale. The CNTs are one-dimensional carbon nanomaterials fillers (1DF's) with single or multiple walls with nanoscale diameters. They have high potential in thermoelectric applications. It is noted that the available trials allow enhancement of composites with 1DFs with the ZT values of both the doped and the undoped bismuth telluride form matrix. For instance, n-type CNTs are of higher diameter than p-type CNTs, as deciding nanotube diameter. In addition, electric conductivity is also influenced by the nanotube diameter. A CNT film module p- and n-type, consisting of 172 thermocouples, with a 465 mV heat output at 49°C has been developed by Kim et al. (Kim et al., 2014).

Carbon nanotubes (CNT) have a high mobility for transporting electrons, which results in high electrical conductivity; hence are well known for their excellent thermal, electrical and mechanical durability. Composting showed to improve the thermoelectric properties of Bi2Te3 system as highlighted in Kim et al. (2006), either by introducing a different filler, such as graphene similar to Suh et al. (2015) or by introducing micro gold particles similar to Nguyen et al. (2019). The basic goal of this approach is to introduce certain impurities and form a new interface at the grain boundaries that improves the material's capacity to scatter phonons, resulting in a decrease in thermal conductivity. The orientation, distribution, form, structure, amount, size and volume of the composting material can all have an impact on the base material characteristics. As

a result, if the filler size is regulated, it can play a significant role in improving thermoelectric characteristics. Nanomaterials (100nm and less) such as carbon nanotubes (CNT) attend to segregate on grain boundaries, forming a new interface. The more pathways electrons have to travel because of smaller particles, the more likely that low mobility electrons will be filtered out. Because of its capacity to transport electrons, CNT dispersion in the Bi2Te3 system can improve its ability to scatter phonons at grain boundaries or at the interface. According to certain research studies, the distribution of CNTs or fullerene - an allotrope of carbon- has the capacity to boost interfaces and improve microstructure, resulting in an improvement in thermoelectric performance (Gothard et al., 2011; Kim et al., 2013). As a result, introducing CNT to Bi2Te3 should affect the thermoelectric characteristics of the entire system. Increasing the concentration of CNT in Bi2Te3 may result in the thermoelectric material exhibiting the expected properties. The novel method of promoting nanostructured bismuth telluride material may lead to additional improvements in its ZT value. In literature, a ZT value of 1 has been demonstrated for the Bi2Te3 system that is acceptable for commercial applications. The use of solid-state solution methods to introduce non-thermoelectric materials has also been investigated by other studies. Their findings showed that the introduction of materials such as C60 and single-walled carbon nanotubes in very small quantities to the Bi2Te3 bulk matrix system increased the Seebeck coefficient while decreasing the thermal conductivity of the entire system.

The multiwalled carbon nanotubes has been used in doping the Bi0.4Sb1.6Te3 system which demonstrated considerable improvements in mechanical characteristics; however with no effect on ZT value. One of the several attempts to fabricate composites utilizing CNT in recent years, demonstrated unsatisfactory ZT values owing to the nature of the polymer employed, in which the polymer’s large complicated molecular

structure hampered the transport of electrons. To fulfil the comprehensive picture of the grain boundaries and the newly created interface owing to the inclusion of CNT, few studies proposed the examination of CNT/Alloys thermoelectric characteristics. For example, the addition of different weight percentages of CNT into lead telluride (PbTe) systems demonstrated the potential of improving the thermoelectric properties. Doping PbTe alloy with 0.05 percent CNT enhanced its electrical conductivity and Seebeck coefficient. CNTs served as a low energy filter at the potential barrier and a favorable route for high energy electrons in the stated system (PbTe), resulting in an increase in electrical conductivity. The density and weight of the CNT, on the other hand, can have a significant impact on its thermoelectric characteristic and capacity to transport electrons. The ZT value achieved when multi-walled carbon nanotubes (MWCNT) were employed is lowered than the case of single-walled carbon nanotubes (SWCNT) employment both compared to the Zt value of the binary system bismuth telluride. The sign of the Seebeck coefficient, however, shifted from n-type to p-type depending on the SWCNT doping amount and temperature. Another investigation was conducted to determine the density of CNTs depending on their diameter. The density and number of walls of a CNT can have a substantial impact on its capacity as an electron carrier. As a result, it is critical to create Bi2Te3 with increased thermoelectric characteristics that is doped with SWCNT. The SWCNT will be homogeneously disseminated in the Bi2Te3 system, and the ZT values will be carefully investigated to evaluate the effectiveness of SWCNT on the thermoelectric characteristics.

CHAPTER 3: METHODOLOGY

This chapter is divided into two parts; the materials utilized are described in the first part, and the process for producing the SWCNT/Bi2Te3 nanocomposites is introduced in the second part. Furthermore, the high-energy ball milling process and sample fabrication needs are discussed. The next section describes the characterization methods used to evaluate the material's thermal, mechanical, structural, and thermoelectric characteristics. The characterization, in summary, contains the following: XRD (PANalytical, EMPYEAN), SEM (Nano-SEM Nova 450, FEI-USA), and HV (Future-Tech, FM-ARS900) analysis are used to determine the grain size and to ensure the purity and proper preparation of samples. Additionally, to ensure the accuracy of the final product grain size calculation, transmission electron microscopy TEM (FEI TitanTM 60-300) is used on one of the composite samples. Additionally, Raman spectroscopy (Thermo Fisher, DXR) is used to characterize both the pristine milled sample and the CNT composites. Raman spectroscopy is used to verify the crystallinity of the carbon nano tube following milling and to investigate the effect of milling time on the structural stability of SWCNT. The thermoelectric characteristics of the improved $Bi_2Te_{2.55}Se_{0.45}$ alloy and the final CNT/ $Bi_2Te_{2.55}Se_{0.45}$ composite samples are investigated using the prepared discs. Measurements are made on the Seebeck coefficient and electrical conductivity utilizing the SBA 485 Nemesis instrument (NETZSCH); in comparison, thermal conductivity is determined using the LFA 467 Hyper Flash instrument (NETZSCH). All of these characterization approaches contribute to adjusting the CNT concentration and time of addition to the $Bi_2Te_{2.55}Se_{0.45}$ alloy. They also contributed to a better understanding of CNT ability to alter the Seebeck coefficient, as well as its electrical, thermal, and mechanical properties, so achieving the research's goal.

3.1 Materials and Methods

Stoichiometric ratios of high purity elements of Bismuth (Bi) (99.99 purity), Tellurium (Te) (99.99% purity) and Selenium (Se) (99.5% purity) are used in order to produce $Bi_2Te_{2.55}Se_{0.45}$ alloy for mechanical milling by using SPEX milling device and milling vial under argon atmosphere. Different SWCNT concentrations are used to optimize the content (0.01, 0.025, 0.1, 0.5 Wt. percent) and added to the pristine in the mixing stage of the process. All these steps help in understanding the structural and thermal stability of CNT and optimizing addition into the alloy.

3.1.1 Samples Preparation with Different CNTs Amounts

Bismuth metal powder (99.99 percent pure, 9.75 g/cm3) with Se metal powder (99.5 percent) and Tellurium (Te) metal powder (99.99 percent pure, 7.74 g/cm3) are obtained as starting materials. The powders serve as a foundation material for incorporating single-walled carbon nanotubes (SWCNTs) into the alloy. To optimize the content, several concentrations of SWCNT (0.01, 0.025, 0.1, 0.5 Wt. percent), sourced from Sigma Aldrich, are introduced to the base metals early in the mixing process. The powders are weighed in a controlled environment chamber (mBRAUN) using ultra-high purity Argon gas (Figure 7).

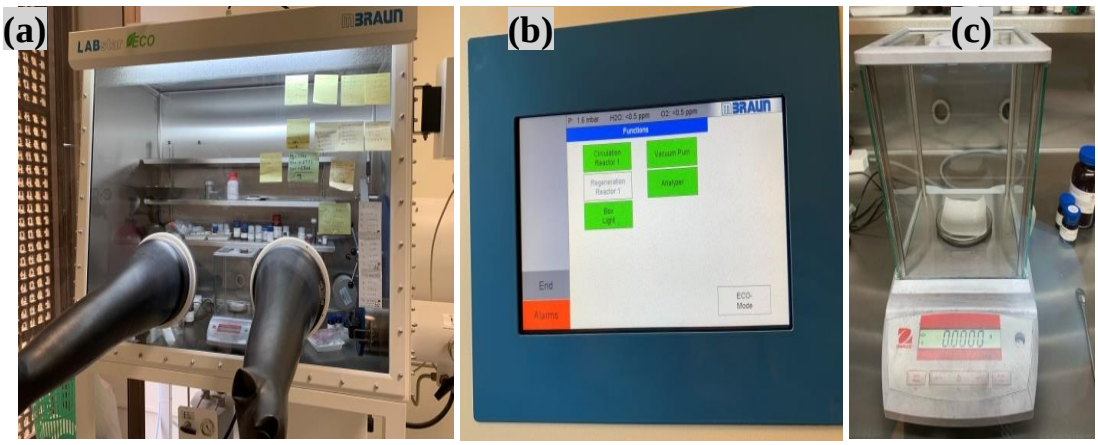

Figure 7: The mBRAUN-LABstar (a) Glovebox workstation and (b) its touch panel (c) along with Ohaus balance weighing equipment.

Equation 11 was used to determine the accurate weight in grams (g) of bismuth, telluride, and MWCNT in order to calculate the correct quantities of the starting material.

$$wt\%(x)_A = \frac{(AT\%(A) * (MW)_A)}{(AT\%(A) * (MW)_A + AT\% * (MW)_B)} x100 \quad (11)$$

Where wt.% is the weight percentage, at% is the atomic weight of each material, and MW is the molecular weight of the pure powders. The aforementioned equation is summarized in Table.1 for both bismuth and tellurium weighing measurements. The aggregate weight of the materials was 5g.

Table 1: The Final Measurements in Grams for Pristine Sample

Element	MW	at%	wt%	Grams
Bi	208.98	40.0	53.7	2.7
Te	127.60	51.0	41.8	2.1
Se	78.96	9.0	4.6	0.2
Total		100.0	100.0	5.0

Table.2 summarizes the final weighing measurements of SWCNT after all the calculations required are done. The different weight fraction of SWCNT is used (0.01, 0.025, 0.1, 0.5 Wt. percent), in which the molecular weight of SWCNT used is 12.1 g/mole.

Table 2: The Final Measurements in Grams for SWCNT/Bi2Te2.55Se0.45 Samples

	Element	MW	at%	wt%	Grams
Bi2Te2.55Se0.45 (0.01)	Bi	208.98	40.0	53.7	2.7
	Te	127.60	51.0	41.8	2.1
	Se	78.96	9.0	4.6	0.2
	CNT	12.01		0.01	0.0005
	Total		100.0	100.0	5.0
Bi2Te2.55Se0.45 (0.025)	Bi	208.98	40.0	53.6	2.7
	Te	127.60	51.0	41.8	2.1
	Se	78.96	9.0	4.6	0.2
	CNT	12.01		0.025	0.0013
	Total		100.0	100.0	5.0
Bi2Te2.55Se0.45 (0.1)	Bi	208.98	40.0	53.61	2.7

	Te	127.60	51.0	41.73	2.1
	Se	78.96	9.0	4.557	0.2
	CNT	12.01		0.1	0.005
	Total		100.0	100.0	5.0
	Bi	208.98	40.0	53.39	2.7
	Te	127.0	51.0	41.57	2.1
Bi2Te2.55Se0.45 (0.5)	Se	78.96	9.0	4.539	0.2
	CNT	12.01		0.5	0.025
	Total		100.0	100.0	5.0

Based on the below measurements in Table 2, each composition powder material was weighted and subjected to the ball milling process.

3.1.2 Compaction of Powdered Samples

All powders samples were compacted using COMPAC technique at 300 ºC and 0.5 GPa for five minutes as holding time (as illustrated in Figure 8). The temperature was selected based on a Bi2Te3 melting point of 580 ºC (Ju & Kim, 2016). It is critical to ensure that sintering occurs below the material's melting point of bismuth telluride to allow for atom diffusion bonding. Additionally, an excessive pressing pressure is employed to make sure nanostructured bulk product has very low porosity, ensuring that the Thermoelectric Property electrical conductivity (σ) is not impaired.

Figure 8: The vacuum hot press system used to compact the processed powders.

3.2 Characterization

Characterization techniques and devices commonly used in the Materials Science field are essential in order to confirm and verify whether the manufactured product is correctly prepared and able to meet its primary or original purpose. In the field of material science, there are many standard methods or tools that are widely used it to analyze, research, measure, determine and understand the concept structure and properties of materials. The techniques for characterization which will be applied in this thesis analysis are detailed in the following subsections.

3.2.1 Structural characterization

3.2.1.1 XRD

X-ray powder diffraction is an application most known for the determination of crystal structure of unknown crystalline materials such as inorganic compounds and measurement lattice parameters of the pre-synthesized nano powder sample such as average grain size and strain calculations as well as minerals. As the technique is mostly used for phase determination of crystalline material and average spacing between the layer of atoms, it can supply data on unit cell dimensions. As a method, X-ray diffraction (XRD) is attractive owing to its quickness and simplicity of performance and because it demands small amount of material, non-destructive and can be used to determine of poly-mineralic mixtures, amorphous, single, and poly materials. Basic principles of (XRD) are established on constructive imbrications of monochromatic X-rays and crystalline specimen. A cathode ray tube, distilled to generate monochromatic radiation, collimated toward the sample, produces these X-rays. The reaction of the rays with sample generates constructive interference when conditions suit Bragg's law ($n\lambda=2d \sin \theta$) (see Figure 9). XRD technique is derived from Bragg's law which states that when the diffracted path difference of the x-rays from two adjacent lattice planes

is equal to multiple of the x-ray wavelength, constructive interference occurs, the law reports the diffraction angle and the lattice spacing with wavelength of electromagnetic radiation in a crystalline specimen. The powder material sample can be detected, counted by scanning between stretch of 2θ angles and all diffraction direction are obtained. Transformation of the diffraction peaks to d-spacing will determine the mineral and this can be done through comparing d-spacing with standard reference patterns. With individualized techniques, XRD can be used to identify crystal structure by Rietveld refinement, identify dislocation density by measuring rocking curve and can be used to identify the thickness, hardness, and density of the film by X-ray reflectivity measurement. For example, in polycrystalline sample can function structural measurements (Deceased & Stock, 2001; Dutrow & Clark, 2012).

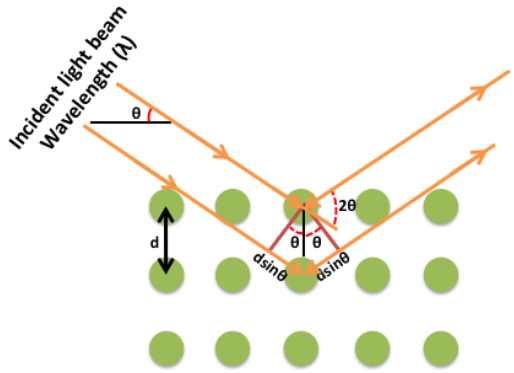

Figure 9: XRD relation with Bragg's law

The purpose of this experiment is to explore and characterize two unknown samples in order to determine the crystal structure type and parameters of the two samples.

EMPYREAN XRD instrument from PANalytical was used to explore and characterize SIX samples. X-ray diffractometers mainly have three components: X-ray tube, sample holder and detector. The x-ray using alpha Copper (Cu Kα1), will hit the filament to yield accelerated electrons into the samples with wavelength of (λ) 1.5404 Å. The detector and sample are moving together as rotation generating an intensity that

is recorded by the reflected x-rays. When the generated geometry satisfies Bragg equation, a constructive interference is indicated and a peak in intensity is generated, as illustrated in Figure 10. The features of X-ray Diffractometer include a computer to control the automatic operation, and the big angle range. Others like accelerating voltage, electron probe current, and a detector.

The operation conditions of the experiment require a 40mA voltage, a range of the Bragg angle from 20^{o} to 70^{o}, and a diffraction speed of 0.7 degree per minute. After specifying these conditional parameters, a little amount of the sample is placed on a glass holder and inserted in the XRD machine.

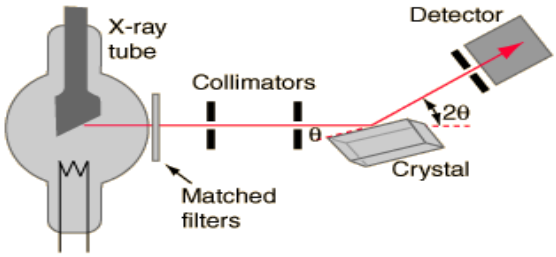

Figure 10: XRD mechanism

3.2.1.2 SEM

NOVA NANOSEM 450 (N-SEM) and energy dispersive spectrometer EDS respectively were used to assess surface morphology and elemental analysis. SEM works basically by ejecting electrons from electron source (electron gun) as (Figure 11). The electrons travel in beams through the column until it reaches the sample. The electron beam travels from the source and focused on the sample to produce secondary electrons and X-rays, which are detected by the detectors resulting in the generation of high quality images There is a 10 mm distance between the sample and the electron source with an applied voltage between 500 V to 30 kV. This voltage is enough to get high quality images at high magnification and it is satisfactory to study the surface morphology. When electrons interact with the sample, secondary electrons and

characteristic X-rays are produced and detected by special detectors. By this electrons image and elemental spectra are produced.

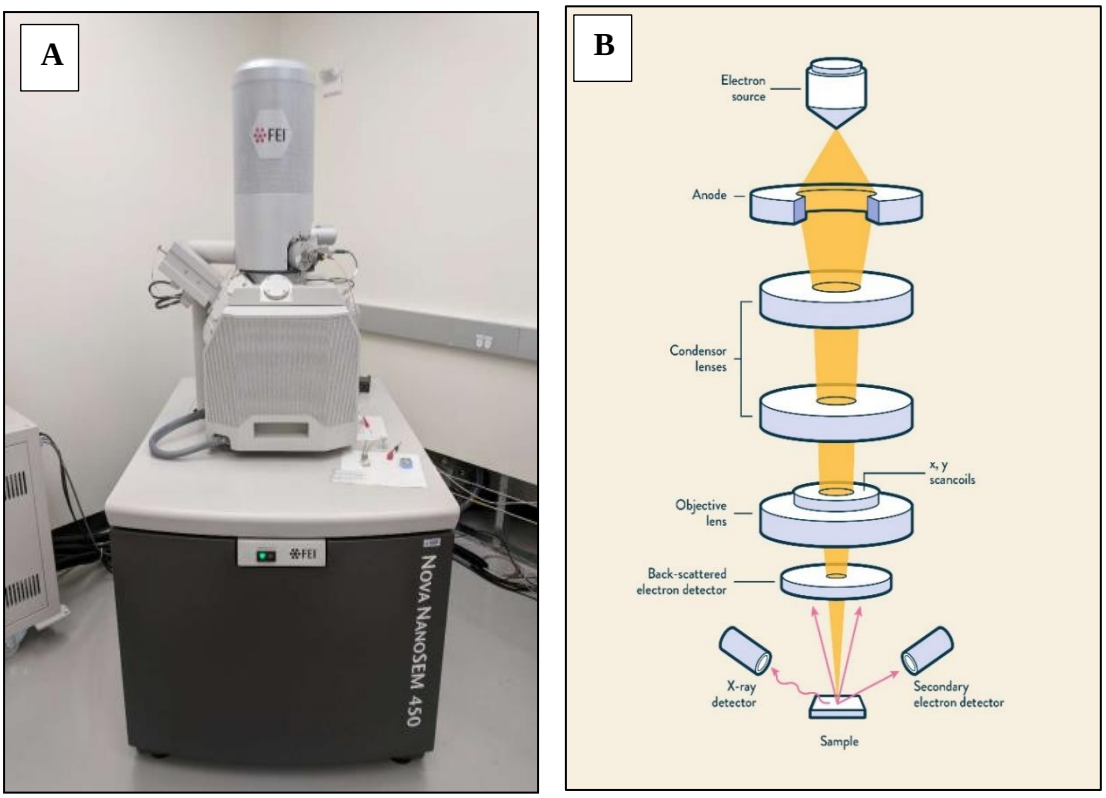

Figure 11: (A) NOVA NANOSEM 450 (N-SEM) instrument (B) SEM Microscope closer look.

3.2.1.3 TEM

TEM is a type of electron microscope where electron beam travels through the sample to study the sample's internal structure. TEM uses a high voltage compared to SEM, thus it provides images with higher magnification and resolution. For this thesis the produced materials were characterized using Talos Transmission Electron Microscope (FEI). For imaging, each sample (very thin layer) was placed in carbon coated grid. While the microscope was operated at 200kV, the sample was positioned on electron beam produced from the electron source. Electrons were focused to penetrate the sample using electromagnetic lenses (see Figure 12). The electron beam travels from the source and focused on the sample to produce high quality images.

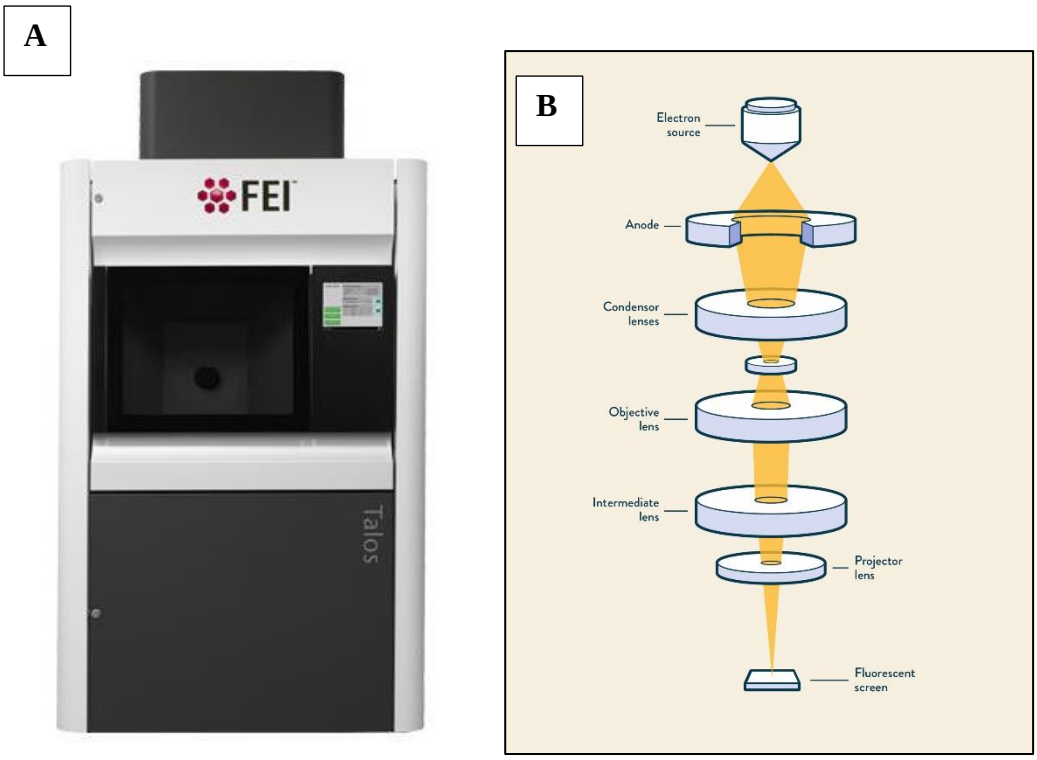

Figure 12: (A) Talos Transmission Electron Microscope (FEI) instrument (B) TEM Microscope closer look.

3.2.1.4 Raman

The Raman microscope is a sophisticated, highly accurate, and non-destructive analytical microscope used to study the crystal structure of many new materials. Thus, the Thermo Scientific DXR Raman microscope was employed to characterize the embedded Carbon nanotubes that serve as fillers in the metallic matrix of BiSlTe, as illustrated in Figure 13.

Figure 13: The Thermo Scientific DXR Raman microscope

The instrument aids in the identification of elements/molecules in TE samples by providing a fingerprint for each element based on its Raman spectrum. The fundamental concept underlying this technique is depicted in Figure 14. Essentially, excitation of electrons within a TE sample using light energy (e.g., phonons) results in Raman scattering, which produces emission at frequencies distinct from the incoming frequency. Stroke lines are those that are created when the frequency of the emitted light is less than the frequency of the incident light, whereas anti-stroke lines are those that are formed more frequently. The TE sample molecule can be identified by examining these distinct stroke and anti-stroke lines for each element. Additionally, the intensity of the emissions can be used to determine the concentration of these molecules in the TE sample.

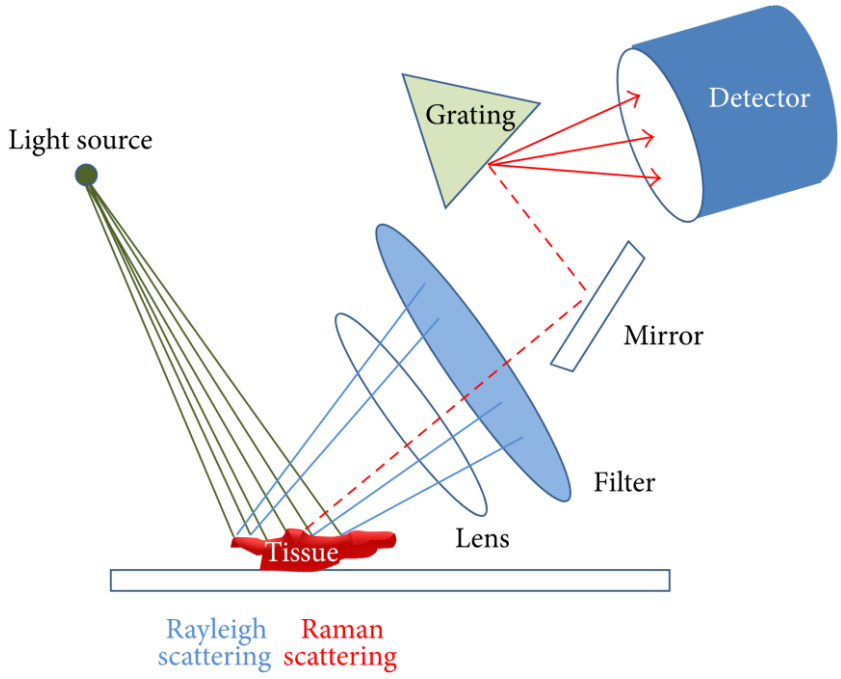

Figure 14: illustrates the Raman spectroscopy basis of operation.

3.2.1.5 Williamson-Hall

Additionally, the peaks produced by an X-Ray Diffraction (XRD) can be utilized to determine the grain size and lattice strain within a unit cell.

Numerous developed methodologies are based on the notion that material processing has an effect on the width and intensity of the peaks. For example, the introduction of strain and the refinement of grain size caused by the mechanical milling process expand and weaken the XRD peaks (Youssef et al., 2006). The models for calculating grain size that were employed in this investigation are described below. The Warren-Averbach approach is based on the use of Fourier series to describe diffraction peaks in order to extract information about grain size of each system and strain. By combining the Cauchy and Gaussian fit of the peaks using Origin-pro analysis software the following equation is obtained:

$$\frac{{\beta_{hkl}}^2}{\tan^2\theta} = \frac{\lambda}{D}\left(\frac{\beta_{hkl}}{\tan\theta\,\sin\theta}\right) + 25\,\langle\varepsilon^2\rangle \qquad (11)$$

where D denotes grain size, ε is indeed the strain, and βhkl is denotes the width of the half-maximum intensity peak (Youssef et al., 2006) building linear relationships using data points over peaks to the $\left(\frac{{\beta_{hkl}}^2}{\tan^2\theta}\right)$ versus $\left(\frac{\beta_{hkl}}{\tan\theta\,\sin\theta}\right)$plot produces a slope showing a constant time the strain value squared and the interplanar distance and the y-intercept of a constant divided by it. a y-intercept representing the constant split by the interplanar spacing, as shown in Figure 15.

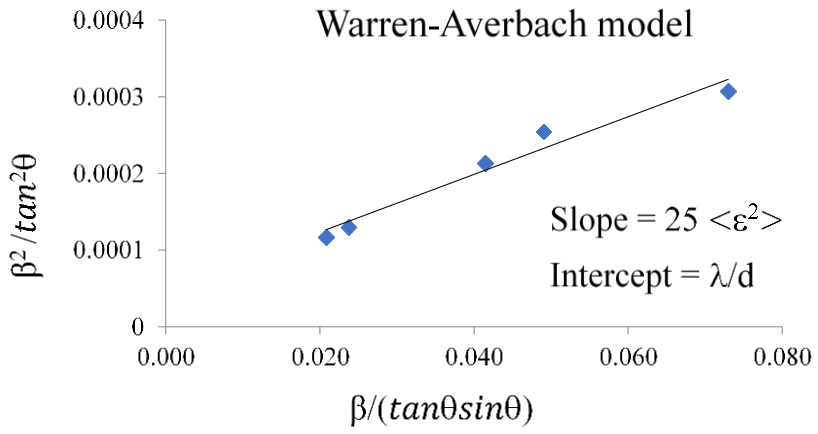

Figure 15: The Warren-Averbach method for calculating grain size.

3.2.2 Mechanical Properties characterization

3.2.2.1 Vickers Hardness

Vickers microhardness is one of the most, standard, frequently, reliable, used nondestructive tests; it is used to determine a sample's mechanical characteristics, specifically Vicker hardness (Hv). The hardness of the material is a characteristic that can endure plastic deformation. The Bi2Te3 alloy (Hv) value depending on several variables, as an example the volume fraction and density of the doped or reinforcing phases (SWCNT). To achieve indentations on the surface of the specimen, the Micro-Hardness Tester instrument, model of FM-ARS9000 utilizes a square trapezium diamond indentor that is operated with a specified force and time, as shown in Figure 16. The depth of these indentations which form a clear square-based pyramid with diagonals of d1 and d2 is then utilized to determine a hardness number using the equation below:

$$\mathrm{HV} = \frac{0.1854\ \mathrm{F(kg)}}{\mathrm{d}^2_{\mathrm{avr}}(\mathrm{mm}^2)} \tag{12}$$

Where Hv denotes hardness number (or Vickers hardness) in MPa, F denotes applied weight/load in N, and d2 is the area of the square-based pyramid indentation in m (Britannica, 2018).

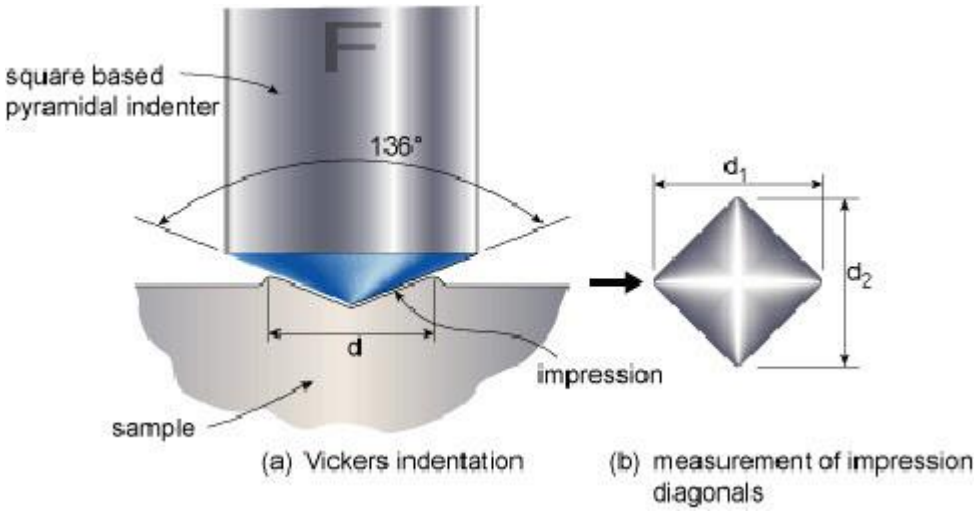

Figure 16: Vickers Micro - hardness schematic representation of the Vickers diamond square-based pyramid that emerged.

3.2.3 Characterization of Thermal Energy

3.2.3.1 Seebeck coefficient and Electrical Conductivity

There are various instruments that may be used to determine the Seebeck coefficient (S) or electrical conductivity (σ) characteristics, but their operation is somewhat different. The gadget used in this investigation is SBA 485 Nemesis' by NETZSCH company. This equipment operates on a four-point system, as seen in Figure 17. The TE sample is positioned between a pair of micro heaters, thermocouples, and current pins in the SBA 485 Nemesis device setup. The Seebeck coefficient which is a ratio of ΔV to ΔT is determined by inducing cyclic heating with the use of microheaters operating in alternation to create a temperature gradient ΔT. This difference in temperature leads in a voltage between the two thermocouples Wires. These voltages ΔV are then measured via thermocouple wires and plotted against the temperature difference ΔT, and the Seebeck coefficient (s) is calculated by the slope of the fitting. Additionally, (σ) is determined by applying varying currents via the two current pins and then measuring the voltage across the sample's two ends.

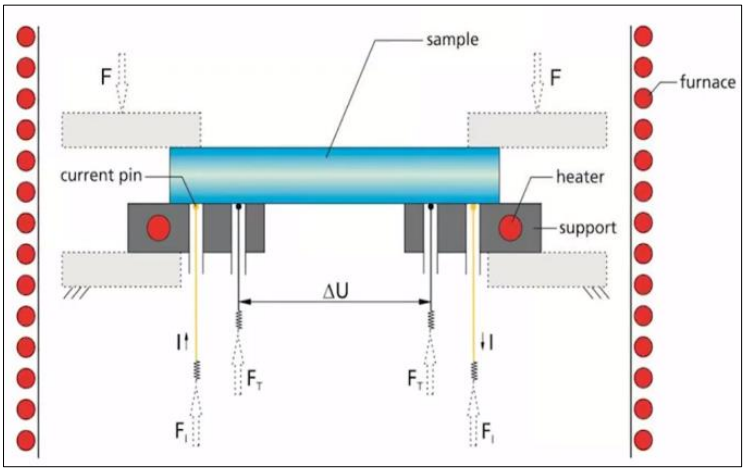

Figure 17: Schematic for the measurement setup of SBA 458 Nemesis device.

3.2.3.2 Thermal Conductivity

The Light Flash Apparatus (LFA) is a valuable tool for determining thermophysical parameters such as thermal conductivity (k) of TE materials. The NETZSCH company 'LFA 467 Hyper Flash' is one gadget that employs this method. adopted Light Flash (LFA) is a non-contact, non-destructive and fast method having a simple operating concept, as illustrated in Figure 18.

Essentially, a light pulse with short energy is used to heat one surface of the thermoelectric sample.

The resulting temperature deviation is then measured using IR detector on the other side, as illustrated in Figures 18 and 19. After measuring the specific heat (Cp), and thermal diffusivity(a), the thermal conductivity (k) is computed as functions of temperature, as follows:

$$\lambda(T) = a(T)\,\rho(T)\,C_p(T) \qquad (13)$$

Where a denotes the thermal diffusivity in mm2/s, ρ denotes the sample density in grams per cubic centimeter, and Cp denotes the specific heat in J/ (g.K).

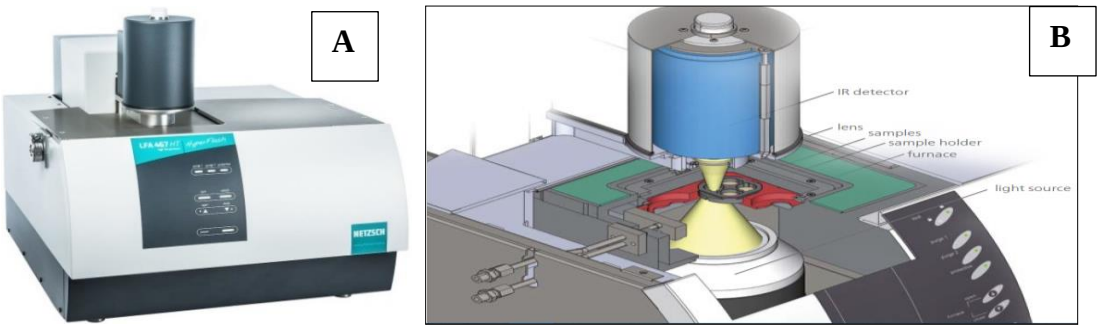

Figure 18: The NETZSCH LFA-467 HyperFlash-Light Flash (a) Apparatus (a) and (b) the entire sample setup.

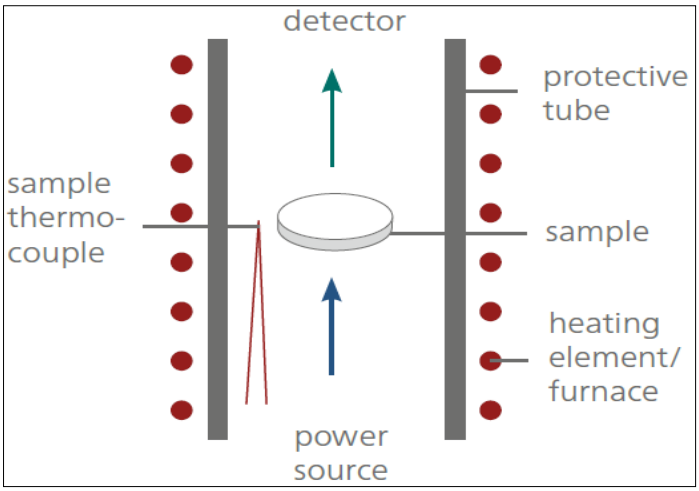

Figure 19: Schematic of the measurement setup for LFA 467 Hyper Flash device.

3.3 Summary of characterization approach

The phases of the millied powdered are identified using X-ray diffraction (XRD: PANalytical, EMPYREAN, United Kingdom) using a Cu/K radiation source and a wavelength of 1.54. Raman Spectroscopy (RS: Thermo Fisher, DXR) is used to determine the degree of crystallinity and structural flaws in SWCNT composite and pristine samples. A wavelength of 532 nm and a laser power of 10 mW are used. Scanning Electron Microscopy are used to characterize the surface morphology and structural characteristics of milled powders (SEM: Nano-SEM Nova 450, FEI company, USA). The microstructure and grain size distribution of the processed TE samples are investigated using transmission electron microscopy (TEM) device. A FEI TitanTM 60–300 TEM is use for the TEM analyses. The TEM sample preparation is carried out utilizing a focused ion beam (FEI Helios NanoLabTM G4 FIB/SEM company) dual system. The Seebeck coefficient and electrical conductivity of the consolidated discs (12.7 mm in diameter and 3 mm in thickness) are simultaneously analyzed by using SBA 485 Nemesis – NETZSCH, Germany. Thermal conductivity is determined using a NETZSCH LFA 467 Hyper Flash instrument. The measurements

for each sample are carried out three times, and the error bar was less than 6 percent on each occasion.

CHAPTER 4: RESULTS AND DISCUSSION

4.1 Surface morphology and composition

4.1.1 X-ray diffraction (XRD)

After completing the mechanical ball milling process for 20 hours under a dry and pure Argon atmosphere with a milling speed of 1080 cycles per minute, the purity of the powders is determined using XRD. X-ray diffraction of doped n-type bismuth telluride results on pristine Bi2Te2.55Se0.45 nano-powders and on Bi2Te3-SWCNT as shown in Figure 20. As indicated in Figure 20, all composites' peaks match and are indexable with the reference code 98-024-7619, indicating that no contamination exists, and the peaks did not shift because of the lengthy milling procedure and that the composition is effectively manufactured. In addition, no SWCNT composite peaks are presented in the diffraction pattern since it is added in small quantity. These results are matching with the literature studies by Ahmad and Wan (2017), Ahmad et al. (2017) and Zhang et al. (2012). Table 3 contains the results from the usage of the Warren-Averbach method of grain size estimation based on XRD data. According to these results, 0.5 % SWCNT shows the lowest grain size for the nano-powders of 16 nm, hence the optimum (amount of SWCNT) milling time.

Table 3: Gran size values for each sample calculated from the XRD analysis.

Sample	Grain size (nm)
0	19.1
0.01	18.3
0.025	18.4
0.1	17.4
0.5	16.0

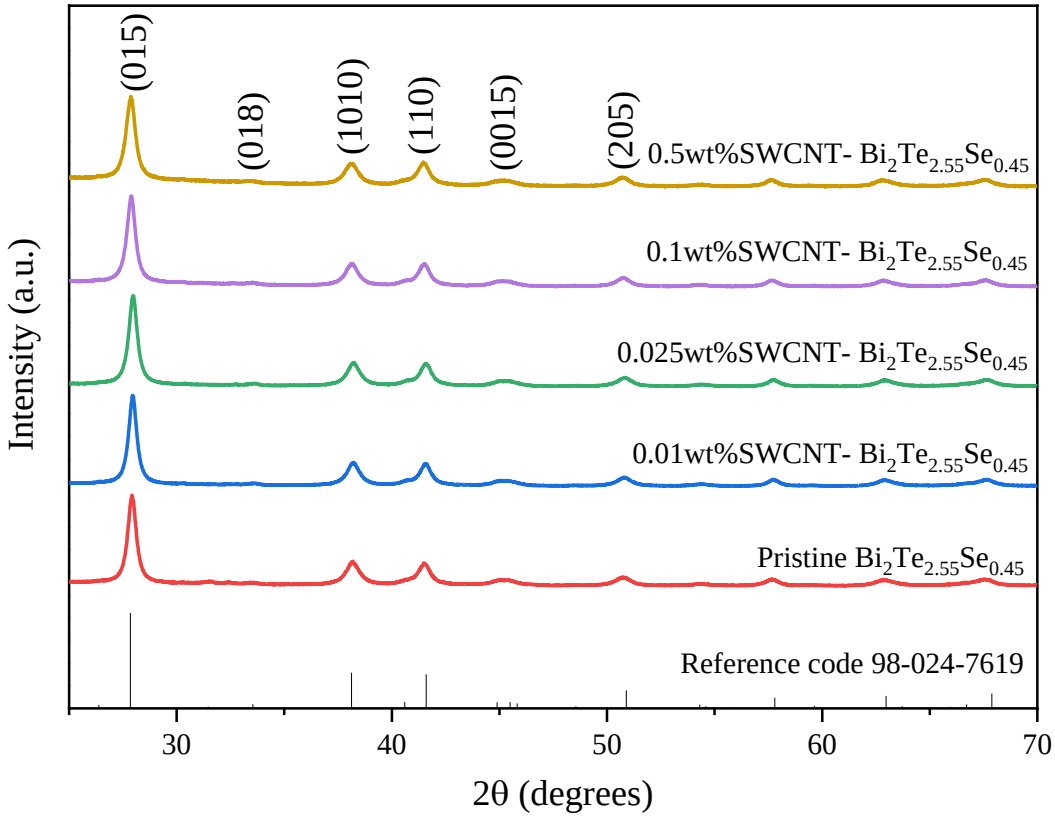

Figure 20: XRD pattern for pristine and SWCNT- $Bi_2Te_{2.55}Se_{0.45}$ composities

4.1.2 Scanning electron microscopy (SEM)

The elemental distribution and the position of the SWCNTs in the material, as well as the grain distribution, were investigated using scanning electron microscopy (SEM). To illustrate the efficacy of the SWCNT and its function in improving the thermoelectric characteristics of Bi2Te3, the following experiments were carried out. SEM microscopy was used to examine the milled alloyed sample's surface morphology and the precise location of CNT within the material.

Figure 21 depicts scanning electron microscopy (SEM) pictures of the morphologies of powder samples that had been milled and of SWCNT. Figure 22

illustrates a typical SWCNT. Figure 21 illustrates the milled powder of pristine $Bi_2Te_{2.55}Se_{0.45,}$ and the 0.5% SWCNT is depicted in the SEM picture in Figure 22. As a result of these studies, The SWCNT was not clearly visible in the three SEM images, which could be attributed to the lengthy 20-hour milling procedure and the extreme plastic deformation that resulted in CNT fragmentation, which caused the SWCNT to be shielded by Bi_2Te_3. Ahmad et al. (2019) investigated the morphology of undoped n-type Gr/Bi_2Te_3 particles and discovered agglomerated particles with distinct graphene nanosheet morphologies. They also identified Bi_2Te_3 particles wrapped in graphene nanosheets. F. M. El-Makaty et al. (2021) reported the same time of ball milling in the 0.05wt%GNP-20 h sample; no nanosheets of GNPs were found due to extreme plastic deformation resulting in GNP fragmentation. Akbar and Youssef (2020) also reported the MWCNT could not be seen clearly in the SEM image. This could be due to the 16-hour milling procedure, which resulted in the MWCNT being shielded by Bi2Te3.

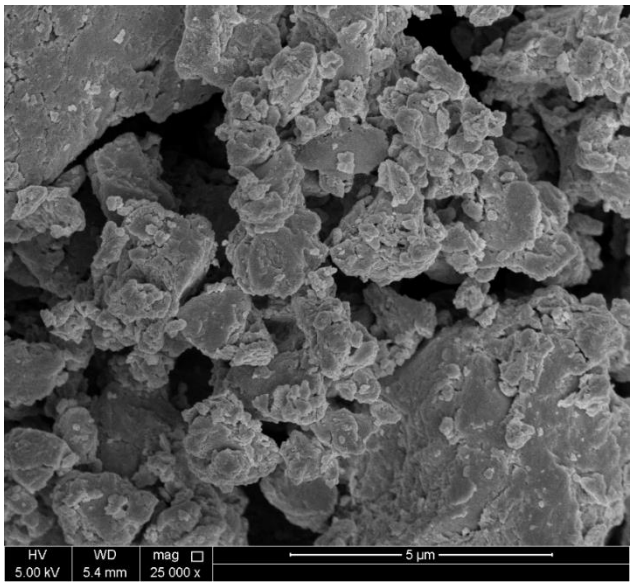

Figure 211: SEM image of pristine sample after milling

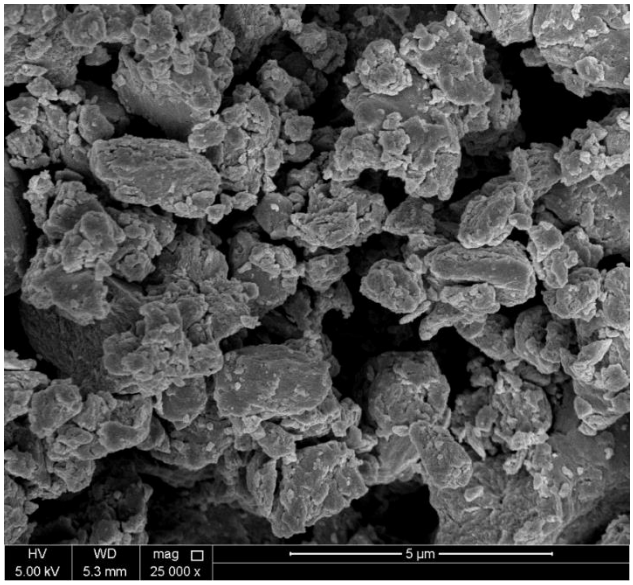

Figure 222: SEM image for Bi2Te3/SWNTs composites 0.5% after milling

4.1.3 Transmission electron microscopy (TEM) analysis

For additional confirmation of the nanocomposites' structure and grain size as determined by XRD. The TEM js utilized to examine the basis material Bismuth telluride and the SWCNT-Bi2Te3 nanocomposite with varying SWCNT contents. The bright-field TEM image of the Pristine sample as milled is shown in Figure 23. The grains are equiaxed and scattered randomly within the structure, as can be observed (Ahmad & Wan, 2017). The bright-field photos demonstrate that the nanograins have sharp grain boundaries, which is consistent with the scale of 100 nm. The average grain size was determined using a dark-field transmission electron microscopy image (see Figure 24) that depicts the corresponding grain size distribution (see Figure 25). From the TEM image in Figure 24, the formation confirms the presence of SWCNT as a thin layer.

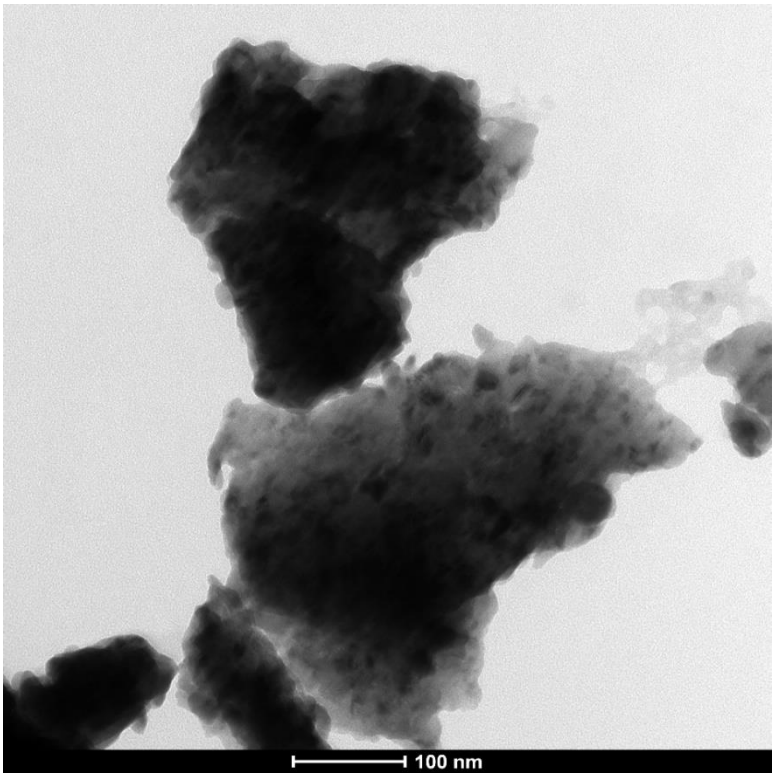

Figure 233: Bright -field TEM image of Bi_2Te_3

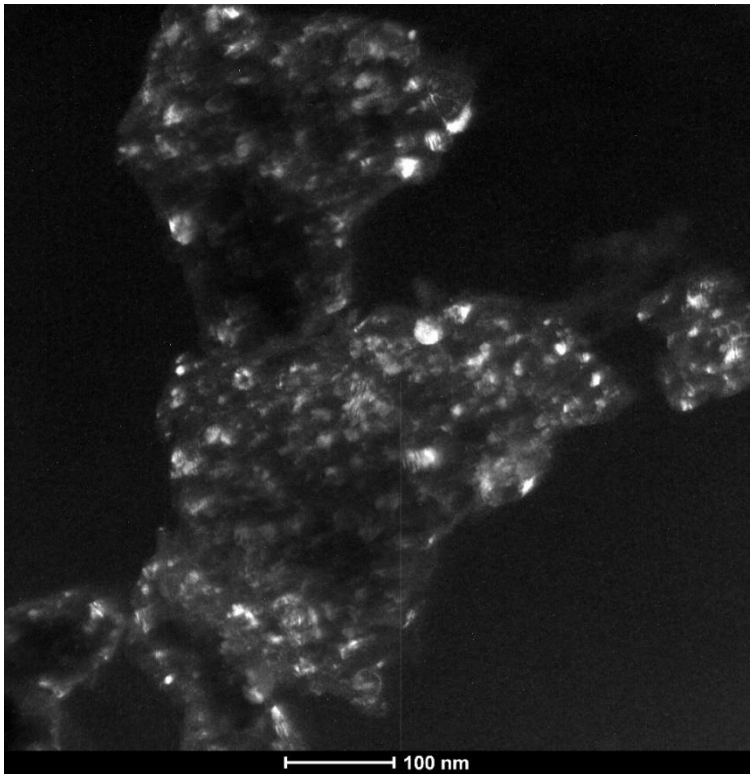

Figure 244: Dark field TEM image of pristine (Bi_2Te_3)

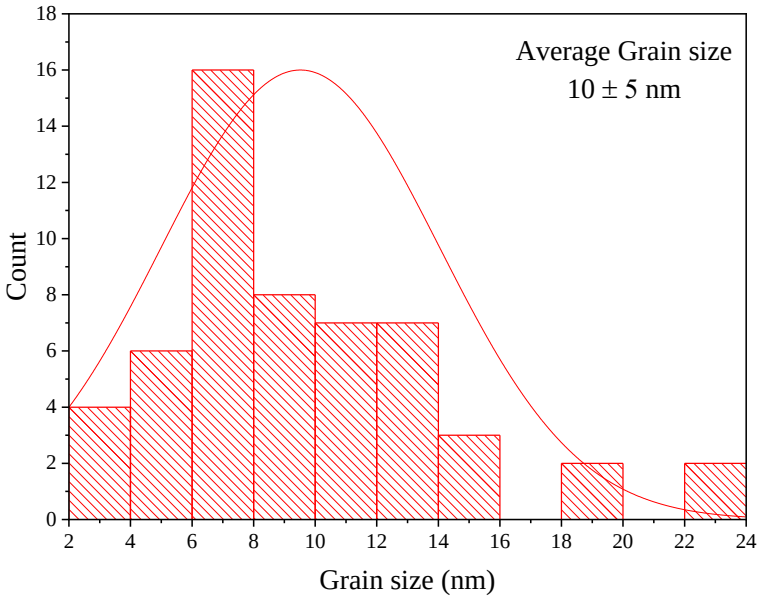

Figure 255: Grain size distribution for pristine sample

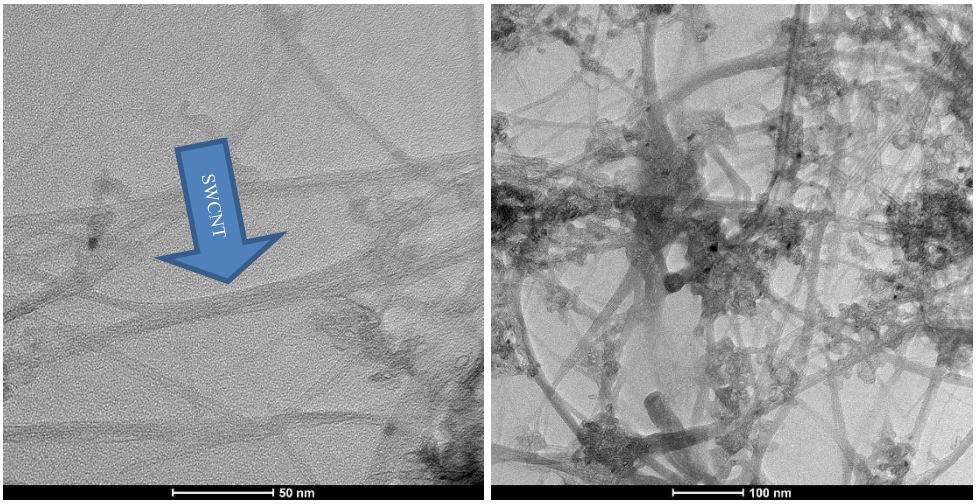

Figure 266: Bright -field TEM image of SWCNT sample

The Pristine sample has an average grain size of 10 ± 5 nm calculated from grains, with no grains larger than 25 nm. This grain size value is comparable to those derived using XRD data of 19 nm. The minor discrepancies in size calculation could be related to the Averbach approach fitting or to the grain selection in the TEM pictures

being ambiguous. However, the uncertainty range is still within reach. As illustrated in Figures 27 and 28, the atomic planes of the pseudohexagonal $Bi_2Te_{2.55}Se_{0.45}$ nanograins are revealed by the electron diffraction pattern, which agrees well with the XRD patterns. From the high-resolution TEM in Figure 28, the interplanar distance is calculated to be 0.315 nm.

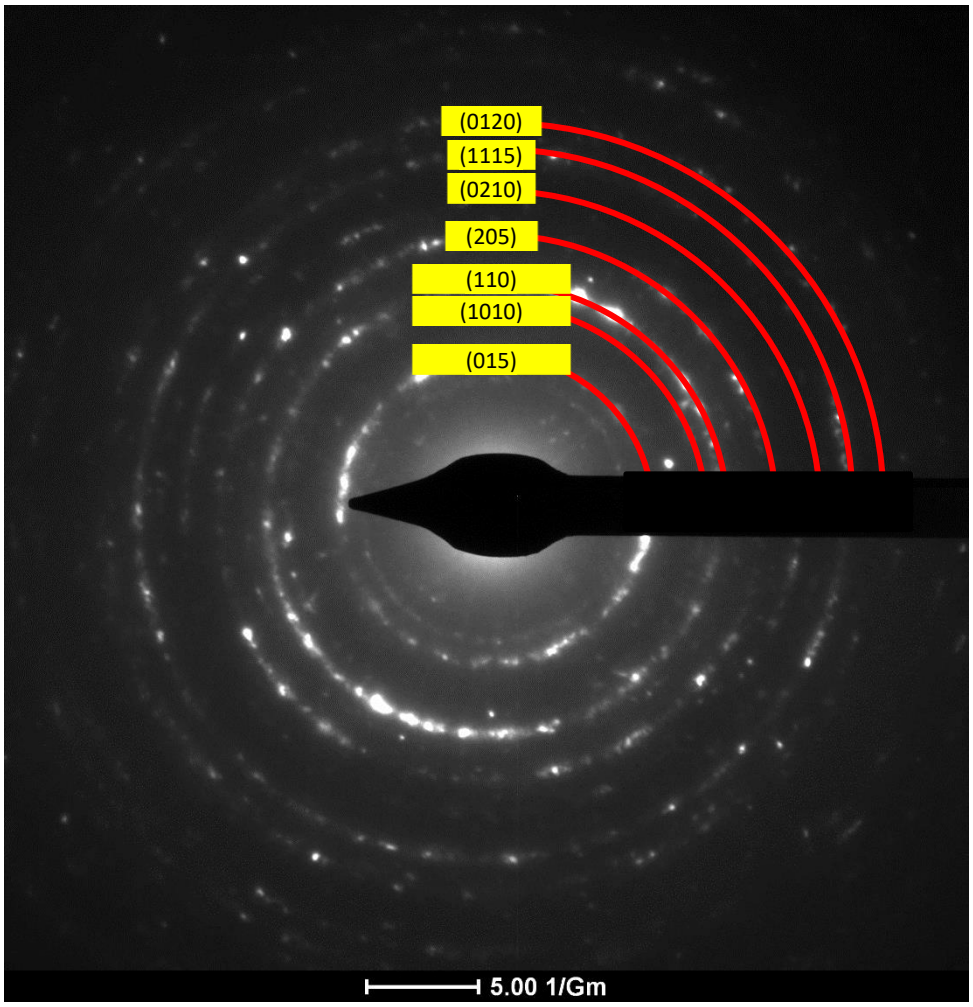

Figure 277: Diffraction pattern for as milled prisitne sample

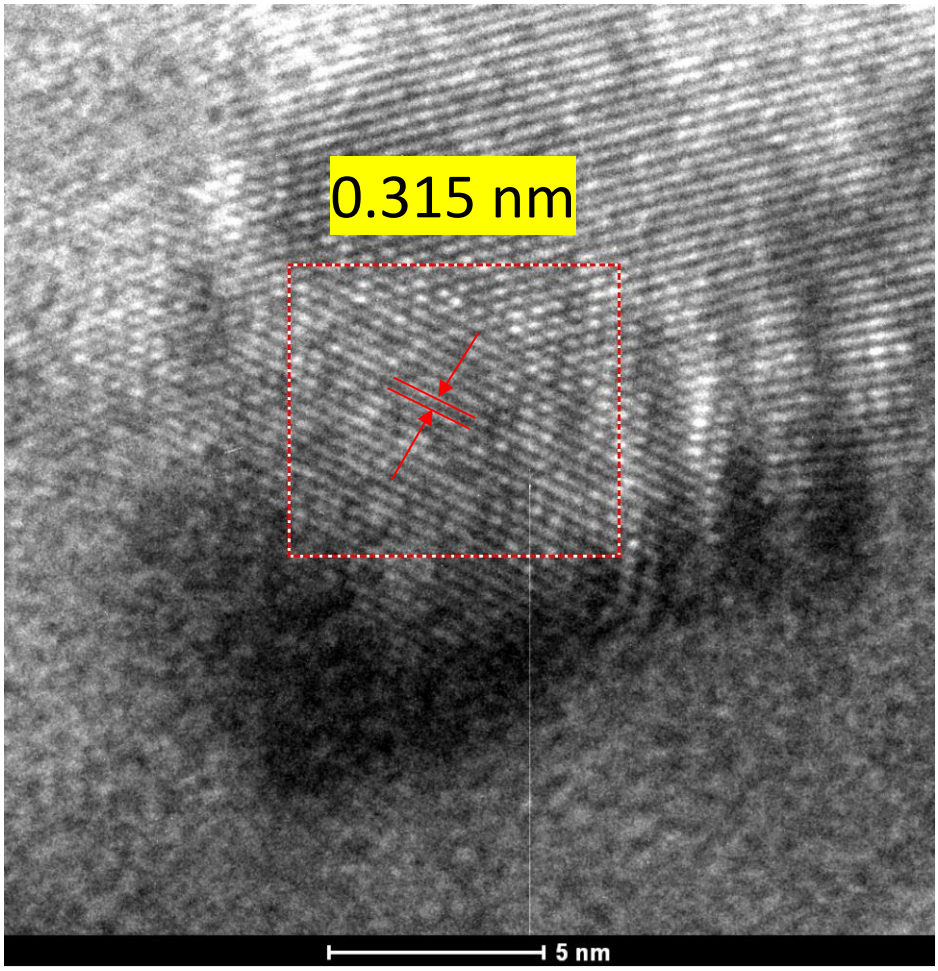

Figure 28: TEM image at high resolution illustrating the interfaces for as milled pristine sample

4.1.4 Raman

Raman spectroscopy was used to investigate the structural changes of the SWCNT in the milled samples in greater detail. The Raman spectroscopy results for the SWCNT in the composite samples are shown in Figure 29 in comparison to the SWCNT as received.

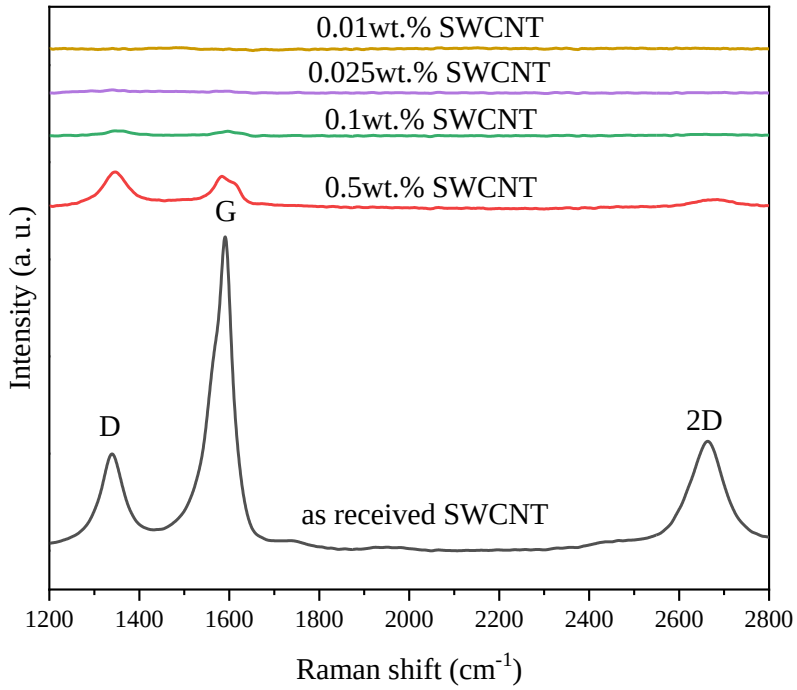

Figure 29: Raman shift of the composite SWCNT - $Bi_2Te_{2.55}Se_{0.45}$ samples.

The G and 2D characteristic bands of SWCNT can be seen in the spectra of the SWCNT materials. The D-band imaging can be used to visualize a single substitutional impurity in the wall of a SWNT 169. The D band is present in 0.5 wt% and 0.1 wt% tested samples except 0.025 wt% SWCNT and 0.01 wt% SWCNT indicating the presence of defects in the carbon lattice of the SWCNT which agree with Kim et al. (2013). The estimated intensity ratio, ID/IG, in Table 4 offers an estimate of the structural integrity of the SWCNT.

Table 4: The intensity ratio of the Raman spectrscopy with different CNT content.

Sample	I_D	I_G	I_{2D}	ID/IG	I2D/IG
SWCNT	248.5	807.7	281.3	0.3	0.35
0.5	82.2	71.0	11.3	1.2	0.16
0.1	32.7	27.1	5.6	1.2	0.21

Generally, the intensity ratio of the D band to the disorder-induced G band, ID/IG, has traditionally been used to determine the size La of a nanocrystal with ordered sp2 C- C bonds or the quantity of localized defects in the sp2 network 65,171–175 (Jorio & Saito, 2021). The ID/IG ratio of SWCNT 20 h implies that the crystal structure of SWCNT has been lost completely. This could explain why SEM analysis revealed no SWCNT. The results demonstrate a clear relationship between the milling time of SWCNT and the structural integrity of the material, with the longer the milling time, the greater the degree of milling-induced structural defects in the product. Since the behavior of CNT varies depending on the technique used to prepare it, these observations are limited to mechanical milling only. ID/IG ratio was higher in the pure sample than composites samples. As a result of a lengthy milling process, there are fragmentation, flaws, and disordering of the SWCNT structure. Another significant trend is visible in the 2D band. The band's strength noticeably decreases as wt % increases, and completely disappears in the high wt% of SWCNT, see Figure 29. This adds to the evidence that SWCNT structural integrity has been compromised because of the high number of defects created during mechanical milling. Additionally, The position of the G band provides more information about the SWCNT doping and strain which can be measured (Jorio & Saito, 2021). The G band increases in Raman energy. The SWCNT -20h and 0.5wt% sample has the greatest change in the G band position, indicating symmetry does not break of SWCNT than the other samples which show symmetry breaking occurs because of a curvature-induced strain in the direction perpendicular to the tube axis, which may be another cause for the lack of SWCNT in the SEM study. the I2D/IG intensity ratio reduces from 0.348 to 0.158, indicating the presence of SWCNT and for 12 hours of milling, SWCNT suffers substantial plastic

deformation (Jorio & Saito, 2021). The ratio then increases to 0.206 for longer milling time implying that SWCNT not exist (Ferrari et al., 2006; Harrison & Atala, 2007).

4.2 Mechanical and physical properties

4.2.1 Hardness test

It is extremely important to understand the mechanical properties of a material since they influence the material's performance and resistance to plastic deformation when it is subjected to high loads and stress. Vickers microhardness testing was performed on samples of pristine and SWCNT-Bi2Te3 nanocomposites. Figure 30 illustrates the hardness values achieved in relation to the SWCNT content. As illustrated in the image, the material's hardness gradually increases as the SWCNT content increases. Which is the anticipated outcome based on the information contained (Bradbury et al., 2014) and also agree with (Akbar & Youssef, 2020) which used MWCNT. Because of the nature of SWCNT, this is an expected effect. The hardness of the base material (Bi2Te3) was determined to be ~ 1.65 GPa, whereas the hardness of the 0.5 wt% SWCNT composite was determined to be ~1.886 GPa. The pristine Bi2Te3 has a lesser hardness than the reinforced Bi2Te3 with SWCNT; this difference can be explained by the empty spaces between the grain bounders and the stress sliding that occurs at such a small size. The rise in hardness values is due to the SWCNT's strong nanostructure and nature, This demonstrates that 20 hours of milling is sufficient to produce Bi2Te2.55Se0.45 nanocrystals with outstanding hardness and nanostructure. SWCNT functions as a barrier at grain boundaries, preventing dislocation motion, slip planes, or defects during stress exposure. It is one of the most often employed strengthening processes in nanostructured materials.

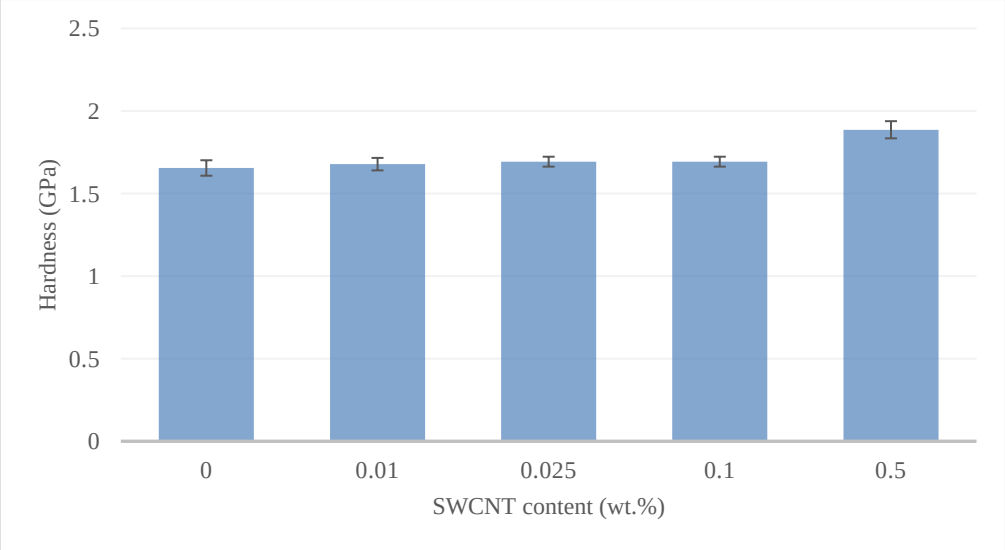

Figure 30: Hardness trend for SWCNT/ Bi2Te2.55Se0.45composites.

4.3 Thermoelectric properties

4.3.1 Electrical conductivity

The electrical conductivity patterns for the consolidated discs of the pristine and TE composite samples are depicted in Figure 31. In this experiment, it is demonstrated that the electrical conductivity increases as the temperature rises. In response to this pattern, the materials demonstrate advanced semiconductor behavior matching with (Fan et al., 2020); Lognoné and Gascoin (2015).

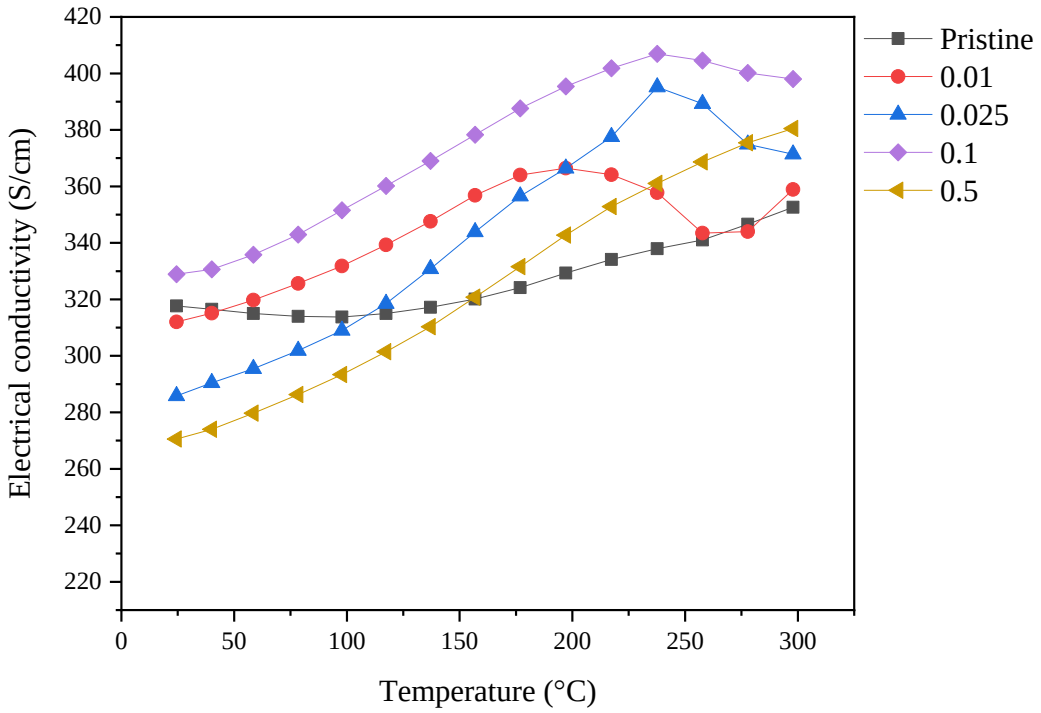

Figure 31: Electrical conductivity of Bi_2Te_3 and Bi_2Te_3-SWCNT nanocomposite as a function of temperature

Comparing the 0.5wt% and 0.025 wt% samples with pristine, which are processed same except for the SWCNT concentration, demonstrates that a lower results in room temperature due to increased carrier scattering at interfaces is caused by a high SWCNT content combined with agglomeration. It has been shown that the induced scattering reduces the mobility of charge carriers and so leads to the lowering of electrical conductivity as agree with F. M. El-Makaty et al. (2021). The electrical property obtained is mostly determined by the amount of SWCNT and its structural integrity. The electrical conductivity of the samples with increase in SWCNT concentration added through ball milling has been improved because of a combined optimization of these two parameters. The higher figure of electrical conductivity is caused by the increase in carrier concentration as well as carrier mobility for the high SWCNT concentration samples as agreed with literature (Kumar et al., 2017).

SWCNT are often a mixture of semiconducting and metallic nanotubes, with a higher proportion of semiconducting nanotubes. As a result, the nonlinear behavior, particularly the decrease in conductivity slope with the addition of SWCNTs in Bi2Te3 with temperature, is seen in samples 0.025 wt% and 0.01 wt% reveals that the electrical transport in the composites is dominated by a thin network of semiconducting nanotubes. Electrical conductivity is proportional to carrier concentration and carrier mobility, and its behavior is generally determined by these two competing factors. This electrical conductivity characteristic is most likely caused by the addition of additional electrons generated by the presence of SWCNT, consistent with previously reported findings and conclusions (Ahmad et al., 2017). Additionally, the 0.1wt% sample has the highest electrical conductivity value at room temperature of 328.9 S/cm compared to pristine. The electrical conductivity of the 0.1 weight percent sample is found to be higher than that of the pristine sample, indicating that the electrical characteristics of the composite were improved as well.

4.3.2 Seebeck Coefficient

Figure 32 displays the Seebeck coefficients for the same samples. Obtaining negative readings indicates that the materials are n-type thermoelectric, where electrons are the primary carriers of charge. Additionally, when temperature rises, the Seebeck coefficient first decrease because of the loss in charge carrier mobility caused by the reduced grain size of the SWCNT then increases until the trend reverses due to the bipolar effect of minority charge carriers. The greatest Seebeck temperature reached by all samples is 156 ^{o}C which agrees well with Kim et al. (2013). The trend obtained for seeback coefficient is consistent with the values reported by Lognoné and Gascoin (2015). Furthermore, as shown in Figure 32, the Seebeck coefficient values for the samples 0.1% SWCNT and 0.025% SWCNT are quite similar over the temperature

range of 25–270 ºC. However, a high concentration of SWCNT in the 0.5 sample results in greater Seebeck coefficient values above 270 ºC, which could be attributable to improved scattering and filtering of high energy carriers. This shows that the increased electrical and Seebeck properties may be due to the 0.5 percent SWCNTs with less agglomeration. When samples containing 0.5 wt percent SWCNT are compared, a direct association between the Seebeck coefficient and the milling duration of the SWCNT is observed. As can be seen in this example, the longer the milling time for the SWCNT is, the greater is the absolute value of the Seebeck coefficient. The Seebeck coefficient is mostly an inherent material characteristic. When SWCNT are milled for an extended period, a greater thermoelectric voltage is induced, a specimen 0.5 SWCNT - 20h. The Seebeck coefficient for SWCNT- $Bi_2Te_{2.55}Se_{0.45}$ can be increased when the structural integrity of the SWCNT is high and there are less defects in the SWCNT, as demonstrated here.

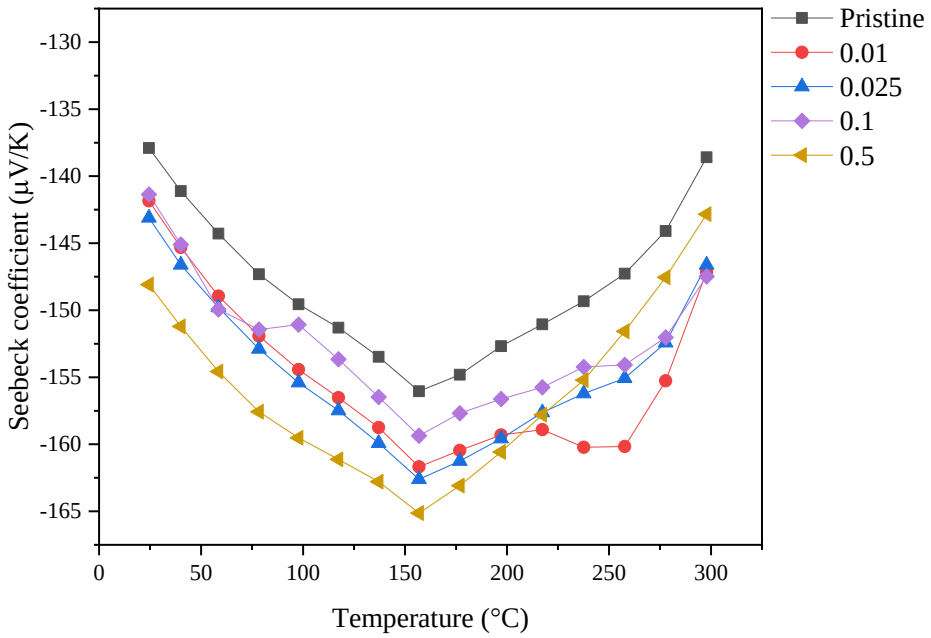

Figure 32: Temperature dependence of the Seebeck coefficient for Bi2Te3 and Bi2Te3-SWCNT nanocomposite

4.3.3 Power factor

In Figure 33, the power factor ($S^2\sigma$), which is derived from structure-sensitive parameters, such as the Seebeck coefficient and electrical conductivity, exhibits a linear temperature relationship. The optimized two TE samples contain a concentration of SWCNT (0.025 and 0.1) applied during mechanical milling. This figure demonstrates that the 0.1wt% nanocomposite has a maximum power factor of 0.97 mW/m.K^2 at 197 ^oC, which decreases gradually to 0.87 mW/m.K^2 at 297 ^oC. These results indicate well agreement with literature reported by Kim et al. (2013) where the maximum power factor of 1.18 mW/m.K^2 is demonstrated at 423 K. However, when compared to pristine $Bi_2Te_{2.55}Se_{0.45}$ sample, 0.5 weight percent sample had a lower value. In addition to having a high-power factor, it also has great mechanical performance.

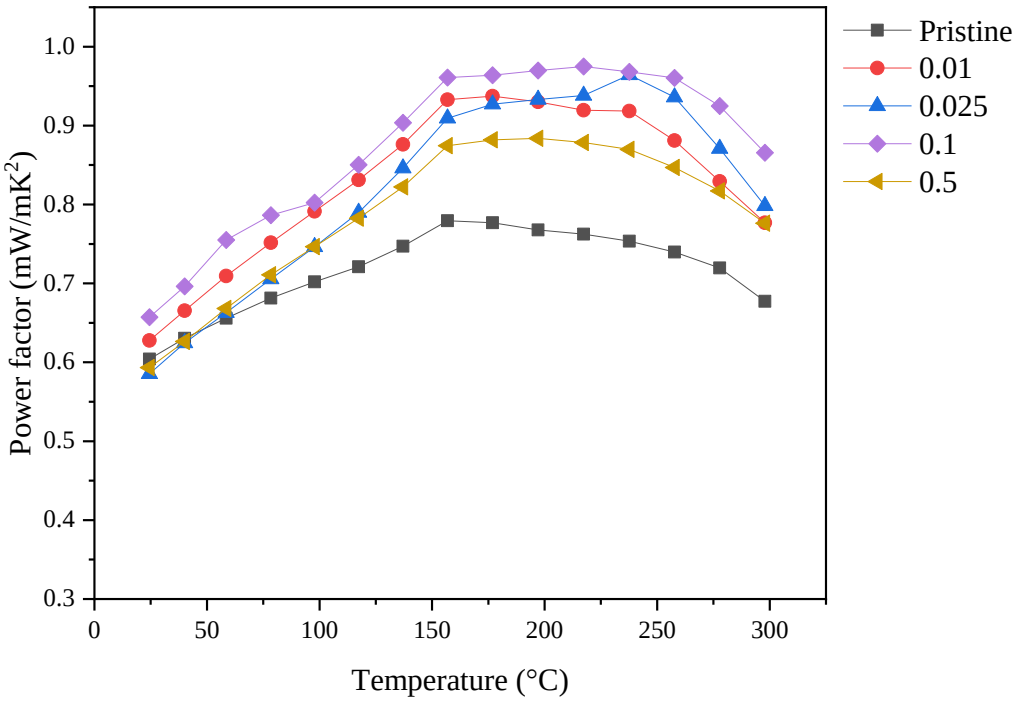

Figure 33: Power factor trends for the pristine and SWCNT/ Bi2Te2.55Se0.45composites samples.

4.3.4 Thermal conductivity

These optimized samples' thermal conductivity is measured and compared to a pristine (Bi2Te2.55Se0.45) bismuth telluride sample. The results are depicted in Figure 34. The overall thermal conductivity values of the two composite samples (0.01 and 0.025 wt%) SWCNT are higher than the values of the pristine sample in this comparison.

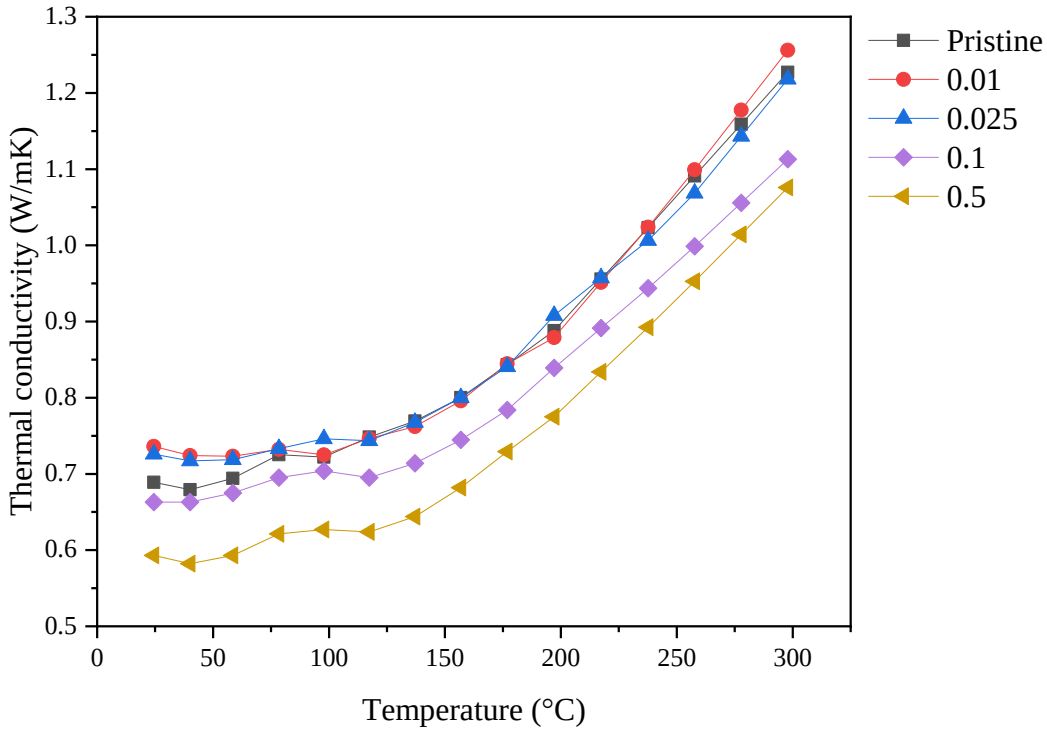

Figure 34: Thermal conductivity of Bi2Te3 and Bi2Te3-SWCNT nanocomposite at different temperatures.

This tendency agrees with the majority of SWCNT-based n-type bismuth tellurides, where SWCNT addition often decreases thermal conductivity due to increased scattering at the new interfaces. The reduction of total thermal conductivity of all composites is caused by the recently formed CNT/$Bi_2Te_{2.55}Se_{0.45}$ interface that

simultaneously creates a lattice phonon dissipation in addition to hot carrier (Kim et al., 2013). It is therefore necessary to calculate a partial influence of the thermal conductivity constituents, which are represented as electronic (κE), lattice vibration (κL), and bipolar (κbipolar) thermal conductivities, on the total effect of the thermal conductivity constituents. Figure 35 illustrates the total thermal conductivity that is obtained by subtracting the electronic component from the lattice and bipolar thermal conductivities (κL+ κbipolar = κTotal - κE) (Kulbachinskii et al., 2011). As given, the overall trend of the lattice and bipolar thermal conductivities is consistent with the findings of other research (Kim et al., 2013). According to Kim and coworkers, liquid-phase sintered bismuth antimony telluride exhibits a significantly reduced lattice thermal conductivity (0.33 W/mK at 320 K) due to strong dispersion of midfrequency-range phonons through dense dislocations at grain boundaries (Kim et al., 2015). Similarly, Poudel et al. (2008) used ball milling technique and hot pressing to create the nanostructured Bismuth telluride composite, and attributed the low thermal conductivity to increased phonon scattering by grain boundaries and defects. This indicated that the inclusion of a nanofiller decreases thermal conductivity due to the substantial increase in phonons scattering at the new interfaces as can be seen in graphene (F. M. El-Makaty et al., 2021). Additionally, the bipolar effect is inhibited across a wider temperature range (up to 300 ^{o}C), indicating that SWCNT can filter out minority carriers (holes) at elevated temperatures. On the other hand, it is likely that the rise in overall thermal conductivity is due to the increase in electronic thermal conductivity. This is mostly because the electronic thermal conductivity component is exactly proportional to the electrical conductivity, which is high in these samples (Figure 36) due to the intact structure of SWCNT and minimal agglomeration.

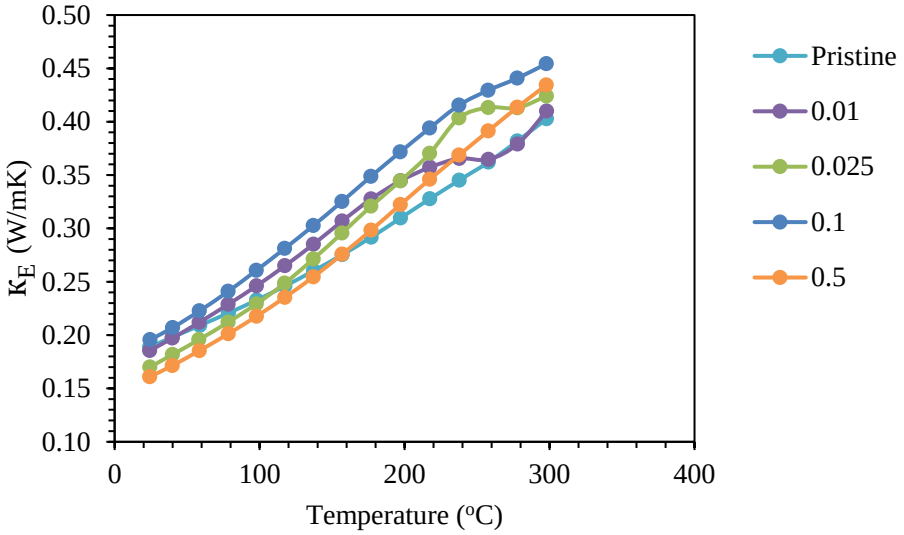

Figure 35: Electronic thermal conductivity of Bi2Te3 and Bi2Te3-SWCNT nanocomposite at different temperatures.

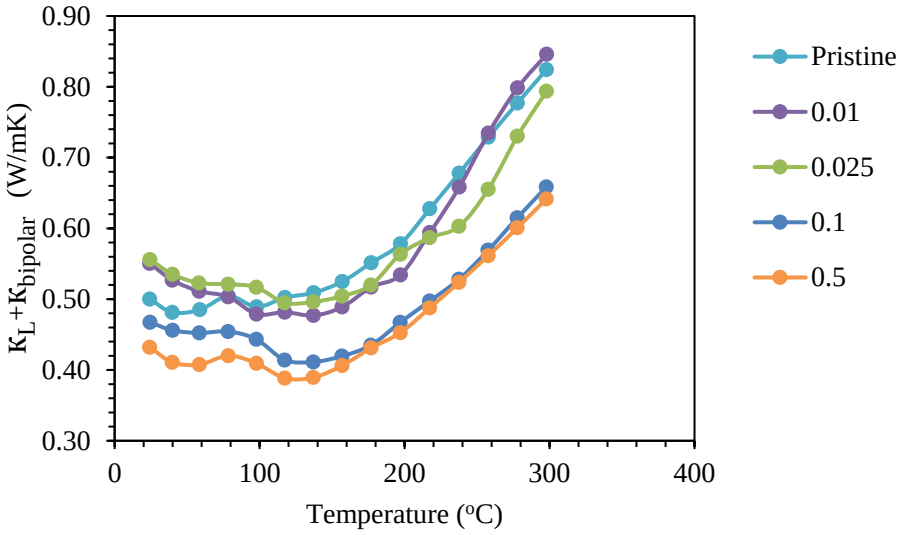

Figure 36: Lattice thermal conductivity of Bi2Te3 and Bi2Te3-SWCNT nanocomposite at different temperatures.

4.3.5 Figure-of-merit

The figure-of-merit, illustrated in Figure 37, demonstrates that the SWCNT-$Bi_2Te_{2.55}Se_{0.45}$ composites exhibit considerable enhancements. As can be observed from graph, the composite samples had greater ZT values than pristine bismuth telluride over the whole temperature range. At room temperature, the inclusion of SWCNT increased the ZT value in the 0.5wt% and 0.1wt% samples to 0.28 and 0.29, respectively. Both values are greater than those for pristine bismuth telluride (0.26). Additionally, the largest enhancement of the ZT values occurred at 150 ºC and reached 0.56 for the 0.1SWCNT sample. This ZT value is approximately 32% higher than that of pure bismuth telluride. When these results are compared to those from prior research that used SWCNT as a filler in conjunction with n-type bismuth telluride, the overall improvement is significantly greater. Kim et al. (2013) demonstrated an improvement from 0.00029 to 0.00035 at a temperature of 75 ºC. Additionally, F. El-Makaty et al. (2021) highlighted the improvement in the ZT figure of merit for Bi_2Te_3 from 0.99 to 1.28 at 282 K with the utilization of 0.5% SWCNT as a filler. Hence, the results confirm that the use of SWCNT in thermoelectric materials, like bismuth telluride, is a potential way of achieving high figures of merit (ZT).

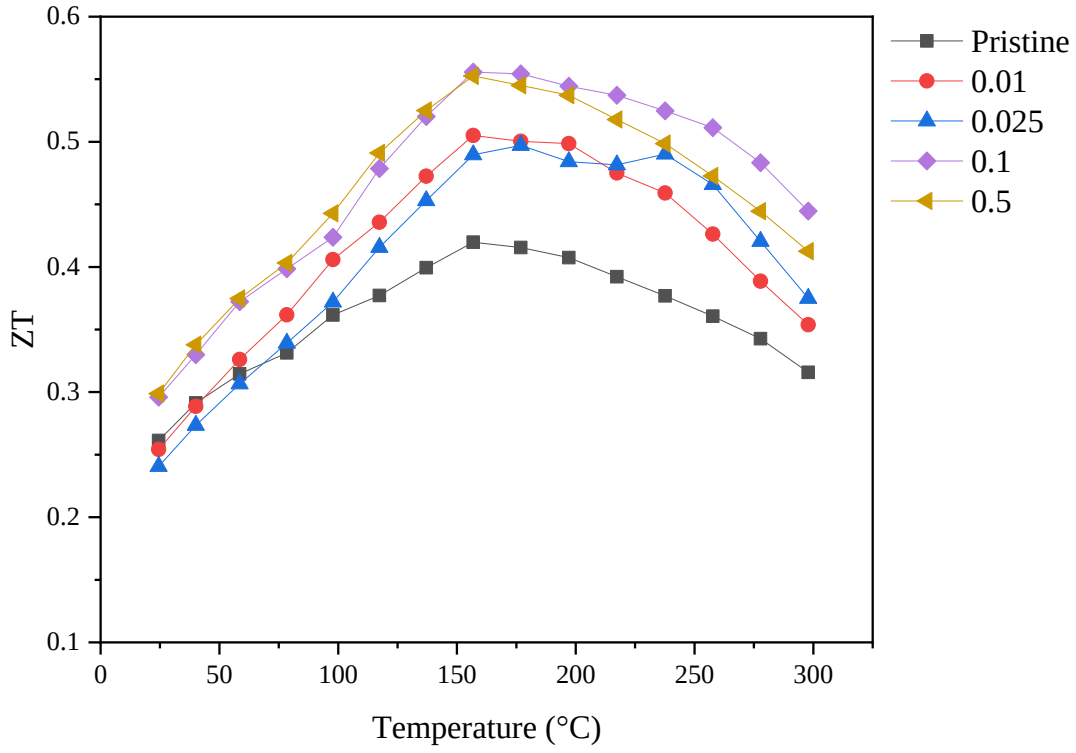

Figure 37: ZT for the SWCNT- Bi2Te2.55Se0.45 pristine and samples.

CHAPTER 5: CONCLUSION

The techniques of ball milling and Compaction sintering are used to create the SWCNT/$Bi_2Te_{2.55}Se_{0.45}$ composite materials. To investigate the effect of SWCNT structural integrity on thermoelectric characteristics, SWCNT are applied at duration time of 20 hours to various SWCNT- $Bi_2Te_{2.55}Se_{0.45}$ samples containing either 0.01, 0.025, 0.1, and 0.5 wt% SWCNT. In accordance with the TEM investigation, it is determined that the average grain size of the milled powders is in the 10 : 5 nm range, with no grains greater than 25 nm. Using a scanning electron microscope, SWCNT are not discovered because of the high plastic deformation that resulted in CNT fragmentation, hence shielding the SWCNT with Bi_2Te_3 in the milled sample after 20 hours. Raman spectroscopy revealed that (i) a longer milling time for SWCNT leads to more milling-induced structural defects, (ii) Calculations of the I2D/IG ratio confirm the critical effect of SWCNT of milling time on its structure, as well as the shape, mechanical behavior, and thermoelectric properties of the produced nanocomposites (iii) With 20 hours milling, the structural integrity of the SWCNT deteriorates or weaken, which explains why no CNT was seen in the SEM study. The thermoelectric properties are significantly influenced by these observations. Due to the no agglomeration and decreased scattering of charge carriers, the electrical conductivity of greater SWCNT concentrations is high. On the other hand, the 20h milling time of SWCNT increased their electrical conductivity by eliminating or reducing the SWCNT structure and high electrical conductivity obtained. With increasing milling time for SWCNT, low structural integrity and excessive defects improved the Seebeck coefficient. Due to the high electrical conductivity of the improved TE samples with less agglomeration, the thermal conductivity of the specimens is dominated by the electronic component. However, due to increased scattering at the new interfaces, a

significant drop in the lattice thermal conductivity is found. In summary, when compared to pristine $Bi_2Te_{2.55}Se_{0.45}$, SWCNT addition increased the ZT value in the composite samples. Due to the structural integrity of SWCNT with low agglomeration, the optimal sample of SWCNT concentration is 0.1 wt% percent milled through mechanical technique increased the figure of merit (ZT) at room temperature to 0.3 (13% higher than pristine) and at 157°C to 0.6 (32 % higher than pristine).

As future work, the potential of optimizing the effect of milling time on the SWCNT structural integrity can be studied by adding the optimized SWCNT (0.1 wt.%) to the n-type bismuth telluride at different milling times. In addition, the possibility to consolidate the optimized composition using a Spark Plasma Sintering (SPS) and compare its thermoelectric properties with the hot compacted samples can be investigated. This can be followed by a detailed TEM analysis of the optimized TE sample along with Hall effect measurements.

REFERENCES

Ahmad, K., & Wan, C. (2017). Enhanced thermoelectric performance of Bi2Te3 through uniform dispersion of single wall carbon nanotubes. *Nanotechnology*, *28*(41), 415402.

Ahmad, K., Wan, C., Al-Eshaikh, M., & Kadachi, A. (2019). Enhanced thermoelectric performance of Bi2Te3 based graphene nanocomposites. *Applied Surface Science*, *474*, 2-8.

Ahmad, K., Wan, C., & Al-Eshaikh, M. A. (2017). Effect of uniform dispersion of single-wall carbon nanotubes on the thermoelectric properties of BiSbTe-based nanocomposites. *Journal of Electronic materials*, *46*(2), 1348-1357.

Akbar, H., & Youssef, K. (2020). The influence of Carbon Nanotubes on the Thermoelectric Properties of Bismuth Telluride.

An, H., Pusko, M., Chun, D., Park, S., & Moon, J. (2019). In-situ synthesis of flexible hybrid composite films for improved thermoelectric performance. *Chemical Engineering Journal*, *357*, 547-558.

Androulakis, J., Hsu, K. F., Pcionek, R., Kong, H., Uher, C., D'Angelo, J. J., . . . Kanatzidis, M. G. (2006). Nanostructuring and High Thermoelectric Efficiency in p-Type Ag (Pb1–ySny) mSbTe2+ m. *Advanced materials*, *18*(9), 1170-1173.

Anno, Y., Takei, K., Akita, S., & Arie, T. (2015). Enhancing the thermoelectric device performance of graphene using isotopes and isotopic heterojunctions. *Advanced Electronic Materials*, *1*(9), 1500175.

Biswas, K., He, J., Blum, I. D., Wu, C.-I., Hogan, T. P., Seidman, D. N., . . . Kanatzidis, M. G. (2012). High-performance bulk thermoelectrics with all-scale hierarchical architectures. *Nature*, *489*(7416), 414-418.

Bradbury, C. R., Gomon, J.-K., Kollo, L., Kwon, H., & Leparoux, M. (2014). Hardness

of multi wall carbon nanotubes reinforced aluminium matrix composites. *Journal of Alloys and Compounds, 585*, 362-367.

Britannica, T. E. o. E. (2018). Vickers Hardness. In *Encyclopaedia Britannica*: Encyclopædia Britannica.

Bulusu, A., & Walker, D. (2008). Review of electronic transport models for thermoelectric materials. *Superlattices and Microstructures*, *44*(1), 1-36.

Chasmar, R., & Stratton, R. (1959). The thermoelectric figure of merit and its relation to thermoelectric generators. *International journal of electronics*, *7*(1), 52-72.

Deceased, B. C., & Stock, S. (2001). Elements of X-ray Diffraction. In: Prentice Hall, USA.

Deng, Y.-G., & Liu, J. (2009). Recent advances in direct solar thermal power generation. *Journal of Renewable and Sustainable Energy*, *1*(5), 052701.

Dresselhaus, M. S., Chen, G., Tang, M. Y., Yang, R., Lee, H., Wang, D., . . . Gogna, P. (2007). New directions for low-dimensional thermoelectric materials. *Advanced materials*, *19*(8), 1043-1053.

Dutrow, B. L., & Clark, C. M. (2012). X-ray powder diffraction (XRD). *Geochemical Instrumentation and Analysis*.

El-Makaty, F., Ahmed, H. K., & Youssef, K. (2021). The effect of different nanofiller materials on the thermoelectric behavior of bismuth telluride. *Materials & Design*, 109974.

El-Makaty, F. M., Mkhoyan, K. A., & Youssef, K. M. (2021). The effects of structural integrity of graphene on the thermoelectric properties of the n-type bismuth-telluride alloy. *Journal of Alloys and Compounds*, *876*, 160198.

Fan, P., Zhang, P.-c., Liang, G.-x., Li, F., Chen, Y.-x., Luo, J.-t., . . . Zheng, Z.-h. (2020). High-performance bismuth telluride thermoelectric thin films fabricated

by using the two-step single-source thermal evaporation. *Journal of Alloys and Compounds*, *819*, 153027.

Fan, S., Zhao, J., Guo, J., Yan, Q., Ma, J., & Hng, H. H. (2010). p-type Bi 0.4 Sb 1.6 Te 3 nanocomposites with enhanced figure of merit. *Applied Physics Letters*, *96*(18), 182104.

Fan, S., Zhao, J., Yan, Q., Ma, J., & Hng, H. H. (2011). Influence of nanoinclusions on thermoelectric properties of n-type Bi 2 Te 3 nanocomposites. *Journal of Electronic materials*, *40*(5), 1018-1023.

Ferrari, A. C., Meyer, J. C., Scardaci, V., Casiraghi, C., Lazzeri, M., Mauri, F., . . . Roth, S. (2006). Raman spectrum of graphene and graphene layers. *Physical review letters*, *97*(18), 187401.

Gayner, C., & Kar, K. K. (2016). Recent advances in thermoelectric materials. *Progress in materials science*, *83*, 330-382.

Goel, M., & Thelakkat, M. (2020). Polymer thermoelectrics: Opportunities and challenges. *Macromolecules*, *53*(10), 3632-3642.

Goldsmid, H. J. (2010). *Introduction to thermoelectricity* (Vol. 121). Springer.

Gothard, N., Tritt, T., & Spowart, J. (2011). Figure of merit enhancement in bismuth telluride alloys via fullerene-assisted microstructural refinement. *Journal of Applied Physics*, *110*(2), 023706.

Harrison, B. S., & Atala, A. (2007). Carbon nanotube applications for tissue engineering. *Biomaterials*, *28*(2), 344-353.

He, M., Qiu, F., & Lin, Z. (2013). Towards high-performance polymer-based thermoelectric materials. *Energy & Environmental Science*, *6*(5), 1352-1361.

Heremans, J. P., Jovovic, V., Toberer, E. S., Saramat, A., Kurosaki, K., Charoenphakdee, A., Snyder, G. J. (2008). Enhancement of thermoelectric

efficiency in PbTe by distortion of the electronic density of states. *Science*, *321*(5888), 554-557.

Hicks, L. D., & Dresselhaus, M. S. (1993a). Effect of quantum-well structures on the thermoelectric figure of merit. *Physical Review B*, *47*(19), 12727.

Hicks, L. D., & Dresselhaus, M. S. (1993b). Thermoelectric figure of merit of a one-dimensional conductor. *Physical Review B*, *47*(24), 16631.

Hsu, K. F., Loo, S., Guo, F., Chen, W., Dyck, J. S., Uher, C., . . . Kanatzidis, M. G. (2004). Cubic AgPbmSbTe2+ m: bulk thermoelectric materials with high figure of merit. *Science*, *303*(5659), 818-821.

Jaldurgam, F. F., Ahmad, Z., & Touati, F. (2021). Synthesis and Performance of Large-Scale Cost-Effective Environment-Friendly Nanostructured Thermoelectric Materials. *Nanomaterials*, *11*(5), 1091. https://www.mdpi.com/2079-4991/11/5/1091

Jorio, A., & Saito, R. (2021). Raman spectroscopy for carbon nanotube applications. *Journal of Applied Physics*, *129*(2), 021102.

Ju, H., & Kim, J. (2016). Preparation and structure dependent thermoelectric properties of nanostructured bulk bismuth telluride with graphene. *Journal of Alloys and Compounds*, *664*, 639-647.

Ju, H., Kim, M., & Kim, J. (2016). Preparation of graphene sheets into one-dimensionally nanostructured bulk bismuth telluride for enhancing thermoelectric power factor. In (Vol. 27, pp. 3427-3434).

Ju, H., Park, D., & Kim, J. (2019). Silicon carbide particles induced thermoelectric enhancement in SnSeS crystal. *Functional Composites and Structures*, *1*(1), 015001.

Kanatzidis, M. G. (2010). Nanostructured thermoelectrics: the new paradigm?

Chemistry of materials, *22*(3), 648-659.

Kasap, S., Koughia, C., Ruda, H., & Johanson, R. (2007). Electrical Conduction in Metals and Semiconductors. In S. Kasap & P. Capper (Eds.), *Springer Handbook of Electronic and Photonic Materials* (pp. 19-45). Springer US. https://doi.org/10.1007/978-0-387-29185-7_2

Kim, K. T., Choi, S. Y., Shin, E. H., Moon, K. S., Koo, H. Y., Lee, G.-G., & Ha, G. H. (2013). The influence of CNTs on the thermoelectric properties of a CNT/Bi2Te3 composite. *Carbon*, *52*, 541-549.

Kim, S. I., Lee, K. H., Mun, H. A., Kim, H. S., Hwang, S. W., Roh, J. W., . . . Lee, Y. H. (2015). Dense dislocation arrays embedded in grain boundaries for high-performance bulk thermoelectrics. *Science*, *348*(6230), 109-114.

Kim, S. L., Choi, K., Tazebay, A., & Yu, C. (2014). Flexible power fabrics made of carbon nanotubes for harvesting thermoelectricity. *Acs Nano*, *8*(3), 2377-2386.

Kim, W., Zide, J., Gossard, A., Klenov, D., Stemmer, S., Shakouri, A., & Majumdar, A. (2006). Thermal conductivity reduction and thermoelectric figure of merit increase by embedding nanoparticles in crystalline semiconductors. *Physical review letters*, *96*(4), 045901.

Kulbachinskii, V., Kytin, V., Blank, V., Buga, S., & Popov, M. Y. (2011). Thermoelectric properties of bismuth telluride nanocomposites with fullerene. *Semiconductors*, *45*(9), 1194-1198.

Kumar, S., Chaudhary, D., Dhawan, P. K., Yadav, R., & Khare, N. (2017). Bi2Te3-MWCNT nanocomposite: an efficient thermoelectric material. *Ceramics International*, *43*(17), 14976-14982.

Kumar, S., Singh, S., Dhawan, P. K., Yadav, R. R., & Khare, N. (2018). Effect of graphene nanofillers on the enhanced thermoelectric properties of Bi2Te3

nanosheets: elucidating the role of interface in de-coupling the electrical and thermal characteristics. In (Vol. 29).

Li, J., Huckleby, A. B., & Zhang, M. (2021). Polymer-based thermoelectric materials: a review of power factor improving strategies. *Journal of Materiomics*.

Lognoné, Q., & Gascoin, F. (2015). On the effect of carbon nanotubes on the thermoelectric properties of n-Bi2Te2. 4Se0. 6 made by mechanical alloying. *Journal of Alloys and Compounds*, *635*, 107-111.

Makongo, J. P., Misra, D. K., Zhou, X., Pant, A., Shabetai, M. R., Su, X., . . . Poudeu, P. F. (2011). Simultaneous large enhancements in thermopower and electrical conductivity of bulk nanostructured half-Heusler alloys. *Journal of the American Chemical Society*, *133*(46), 18843-18852.

Mamur, H., Bhuiyan, M., Korkmaz, F., & Nil, M. (2018a). A review on bismuth telluride (Bi2Te3) nanostructure for thermoelectric applications. *Renewable and Sustainable Energy Reviews*, *82*, 4159-4169.

Mamur, H., Bhuiyan, M. R. A., Korkmaz, F., & Nil, M. (2018b). A review on bismuth telluride (Bi2Te3) nanostructure for thermoelectric applications. *Renewable and Sustainable Energy Reviews*, *82*, 4159-4169.

Manzano, C. V., Abad, B., Rojo, M. M., Koh, Y. R., Hodson, S. L., Martinez, A. M. L., . . . Borca-Tasciuc, T. (2016). Anisotropic effects on the thermoelectric properties of highly oriented electrodeposited Bi 2 Te 3 films. *Scientific reports*, *6*, 19129.

Neeli, G., Behara, D. K., & Kumar, M. K. (2016). State of the art review on thermoelectric materials. *International Journal of Science and Research*, *5*, 1833-1844.

Nguyen, T. H., Enju, J., & Ono, T. (2019). Enhancement of thermoelectric properties

of bismuth telluride composite with gold nano-particles inclusions using electrochemical co-deposition. *Journal of the electrochemical society*, *166*(12), D508.

Nozariasbmarz, A., Poudel, B., Li, W., Kang, H. B., Zhu, H., & Priya, S. (2020). Bismuth Telluride Thermoelectrics with 8% Module Efficiency for Waste Heat Recovery Application. *Iscience*, *23*(7), 101340.

Park, K. H., Mohamed, M., Aksamija, Z., & Ravaioli, U. (2015). Phonon scattering due to van der Waals forces in the lattice thermal conductivity of Bi2Te3 thin films. *Journal of Applied Physics*, *117*(1), 015103. https://doi.org/10.1063/1.4905294

Poudel, B., Hao, Q., Ma, Y., Lan, Y., Minnich, A., Yu, B., . . . Vashaee, D. (2008). High-thermoelectric performance of nanostructured bismuth antimony telluride bulk alloys. *Science*, *320*(5876), 634-638.

Quarez, E., Hsu, K.-F., Pcionek, R., Frangis, N., Polychroniadis, E., & Kanatzidis, M. G. (2005). Nanostructuring, compositional fluctuations, and atomic ordering in the thermoelectric materials AgPb m SbTe2+ m. The myth of solid solutions. *Journal of the American Chemical Society*, *127*(25), 9177-9190.

Rowe, D. M. (2018). *CRC handbook of thermoelectrics*. CRC press.

Shen, Q., Chen, L., Goto, T., Hirai, T., Yang, J., Meisner, G., & Uher, C. (2001). Effects of partial substitution of Ni by Pd on the thermoelectric properties of ZrNiSn-based half-Heusler compounds. *Applied Physics Letters*, *79*(25), 4165-4167.

Shi, X.-L., Zou, J., & Chen, Z.-G. (2020). Advanced thermoelectric design: from materials and structures to devices. *Chemical Reviews*, *120*(15), 7399-7515.

Shin, W. H., Ahn, K., Jeong, M., Yoon, J. S., Song, J. M., Lee, S., . . . Lim, Y. S. (2017). Enhanced thermoelectric performance of reduced graphene oxide incorporated bismuth-antimony-telluride by lattice thermal conductivity reduction. *Journal*

of Alloys and Compounds, *718*, 342-348.

Slack, G. A., & Tsoukala, V. G. (1994). Some properties of semiconducting IrSb3. *Journal of Applied Physics*, *76*(3), 1665-1671.

Suh, D., Lee, S., Mun, H., Park, S.-H., Lee, K. H., Kim, S. W., . . . Baik, S. (2015). Enhanced thermoelectric performance of Bi0. 5Sb1. 5Te3-expanded graphene composites by simultaneous modulation of electronic and thermal carrier transport. *Nano Energy*, *13*, 67-76.

Suryanarayana, C. (2001). Mechanical alloying and milling. *Progress in materials science*, *46*(1-2), 1-184.

Takashiri, M., Takiishi, M., Tanaka, S., Miyazaki, K., & Tsukamoto, H. (2007). Thermoelectric properties of n-type nanocrystalline bismuth-telluride-based thin films deposited by flash evaporation. *Journal of Applied Physics*, *101*(7), 074301.

Tong, X. C. (2011). *Advanced materials for thermal management of electronic packaging* (Vol. 30). Springer Science & Business Media.

Tritt, T. M., & Subramanian, M. (2006). Thermoelectric materials, phenomena, and applications: a bird's eye view. *MRS bulletin*, *31*(3), 188-198.

Xie, W., Tang, X., Yan, Y., Zhang, Q., & Tritt, T. M. (2009). High thermoelectric performance BiSbTe alloy with unique low-dimensional structure. *Journal of Applied Physics*, *105*(11), 113713.

Xie, W., Yan, Y., Zhu, S., Zhou, M., Populoh, S., Gałązka, K., . . . Tang, X. (2013). Significant ZT enhancement in p-type Ti (Co, Fe) Sb–InSb nanocomposites via a synergistic high-mobility electron injection, energy-filtering and boundary-scattering approach. *Acta Materialia*, *61*(6), 2087-2094.

Yang, J., Li, H., Wu, T., Zhang, W., Chen, L., & Yang, J. (2008). Evaluation of half-

Heusler compounds as thermoelectric materials based on the calculated electrical transport properties. *Advanced Functional Materials*, *18*(19), 2880-2888.

Yao, C.-J., Zhang, H.-L., & Zhang, Q. (2019). Recent Progress in Thermoelectric Materials Based on Conjugated Polymers. *Polymers*, *11*(1), 107. https://www.mdpi.com/2073-4360/11/1/107

Youssef, K., Scattergood, R., Murty, K., & Koch, C. (2006). Nanocrystalline Al–Mg alloy with ultrahigh strength and good ductility. *Scripta materialia*, *54*(2), 251-256.

Yu, J., Sun, Q., & Jena, P. (2016). Recent advances in 2D thermoelectric materials. International Symposium on Clusters and Nanomaterials,

Zhang, Y., Ma, H., Sun, B., Liu, B., Liu, H., Kong, L., . . . Chen, X. (2017). Thermoelectric performance of graphene composited BiSbTe bulks by high pressure synthesis [Article]. *Journal of Alloys and Compounds*, *715*, 344-348. https://doi.org/10.1016/j.jallcom.2017.05.004

Zhang, Y., Wang, X., Yeoh, W., Zheng, R., & Zhang, C. (2012). Electrical and thermoelectric properties of single-wall carbon nanotube doped Bi2Te3. *Applied Physics Letters*, *101*(3), 031909.

Zhou, M., Li, J.-F., & Kita, T. (2008). Nanostructured AgPb m SbTe m+ 2 system bulk materials with enhanced thermoelectric performance. *Journal of the American Chemical Society*, *130*(13), 4527-4532.